Origin and Evolution of the Sierra Nevada
and Walker Lane themed issue

Late Quaternary faulting history of the Carrizal and related faults, La Paz region, Baja California Sur, Mexico

Paul J. Umhoefer[1], Sara J. Maloney[1], Beverly Buchanan[1], J Ramón Arrowsmith[2], Genaro Martinez-Gutiérrez[3], Graham Kent[4], Neal Driscoll[5], Alistair Harding[5], Darrell Kaufman[1], and Tammy Rittenour[6]

[1]*School of Earth Sciences and Environmental Sustainability, Northern Arizona University, 625 S. Knoles Drive, Flagstaff, Arizona 86011, USA*

[2]*School of Earth and Space Exploration, Arizona State University, Tempe, Arizona 85287-1404, USA*

[3]*Departamento de Geologia Marina, Universidad Autonoma de Baja California Sur, La Paz, Baja California Sur 23080, Mexico*

[4]*Nevada Seismological Laboratory/0174, University of Nevada, Reno, Reno, Nevada 89557, USA*

[5]*Scripps Institution of Oceanography, 9500 Gilman Drive, University of California, San Diego, San Diego, California 92124, USA*

[6]*Department of Geology, 4505 Old Main Hill, Utah State University, Logan, Utah 84322-4505, USA*

ABSTRACT

The southwest margin of the Gulf of California has an array of active normal faults despite this being an oblique-divergent plate boundary with spreading centers that localized deformation along the plate boundary 2–3 million years ago. The Carrizal and Centenario faults form the western border fault of the Gulf of California marginal fault system within and south of La Paz Bay, and ~20–30 km west of the capital city of La Paz, Baja California Sur, Mexico. Geologic and geomorphic mapping, optically stimulated luminescence (OSL) geochronology, and paleoseismic investigations onshore, compressed high-intensity radar pulse (CHIRP) profiling offshore, and analysis of uplifted marine terraces in the footwall of the offshore Carrizal fault provide some of the first numerical and geometrical constraints on late Pleistocene–Holocene faulting along the Carrizal fault. The onshore Carrizal fault has ruptured with up to ~1–2 m of vertical displacement per event, likely producing ~M 6.3–6.9 earthquakes, and at least two to three surface rupturing earthquakes have occurred since 22 ka. Onshore paleoseismic excavations and uplifted marine terraces on the western side of La Paz Bay both suggest offset rates of 0.1–0.2 mm/yr, with a footwall uplift rate of 0.13 mm/yr since 128 ka, and an approximately constant rate since marine oxygen-isotope stage (MIS) 11 terraces (420 ka). A CHIRP survey identified underwater fault scarps with heights ranging from 21 to 86 m on the Carrizal fault in La Paz Bay and from 3 to 5 m along the Centenario fault. The offshore Carrizal fault lies 8–10 km east of the western edge of La Paz Bay, forming a right step from the onshore Carrizal fault. The offshore Carrizal fault is the oldest fault of the fault system, and the fault likely grew in the latest Miocene to Pliocene in a complex way to the south toward the onshore Centenario and Carrizal faults. When the Alarcon spreading center started its modern rates at 2.4 Ma, the Carrizal fault likely slowed to the 0.1–0.2 mm/yr rates of the late Quaternary determined in this study.

INTRODUCTION

A fundamental process along divergent to oblique divergent plate boundaries is the formation of a rift and the eventual localization of faulting along a discrete boundary. The Gulf of California is an active oblique-divergent plate boundary (Lonsdale, 1989; Plattner et al., 2007) that formed between the North American and Pacific plates (Stock and Hodges, 1989), and has largely localized plate motion in the past 2–3 million years. Despite this fault localization along the dominant plate boundary, faults remain active in the southwestern gulf-margin fault system along the southeastern Baja California peninsula and offshore near the peninsula (Fletcher and Munguía, 2000; Martínez-Gutiérrez and Jorajuria-Lara, 2003; Munguía et al., 2006; Busch et al., 2011). Understanding the relation of the gulf-margin system within the plate boundary as a whole will lead us to better understand the process of localization of faulting at divergent plate boundaries and the rift to drift transition process.

Despite clear evidence from earthquakes that the gulf-margin fault system is active (Fig. 1) (Fletcher and Munguía, 2000), there has been no systematic quantification of the fault slip rates until this and related studies (e.g., Busch et al., 2011; Coyan et al., 2013). The active normal faults in the gulf-margin fault system at the latitude of La Paz include the Carrizal fault, the border fault that runs along the main Gulf escarpment, and 2–3 active fault systems to the east (Figs. 2 and 3). Busch et al. (2011) defined the basic fault patterns and basin geometries of the onshore gulf-margin fault system based on mapping and gravity surveys; and presented preliminary Holocene slip rates of ~0.1 mm/yr along the San Juan de Los Planes fault. A companion study by Busch et al. (now Coyan et al., 2013) summarized the active faulting of the Los Planes basin onshore and offshore east of La Paz 30–50 km.

The present study provides the first quantitative constraints on late Quaternary slip rates along the Carrizal border fault, both onshore and offshore, and contributes to understanding the patterns and rates of active faulting observed along the southwestern Gulf of California plate boundary. The study is also important because the Carrizal fault lies 20–30 km from the major city of La Paz, the capital of Baja California Sur,

Geosphere; June 2014; v. 10; no. 3; p. 476–504; doi:10.1130/GES00924.1; 12 figures; 6 tables; 1 supplemental file.
Received 3 March 2013 ♦ Revision received 4 December 2013 ♦ Accepted 24 February 2014 ♦ Published online 10 April 2014

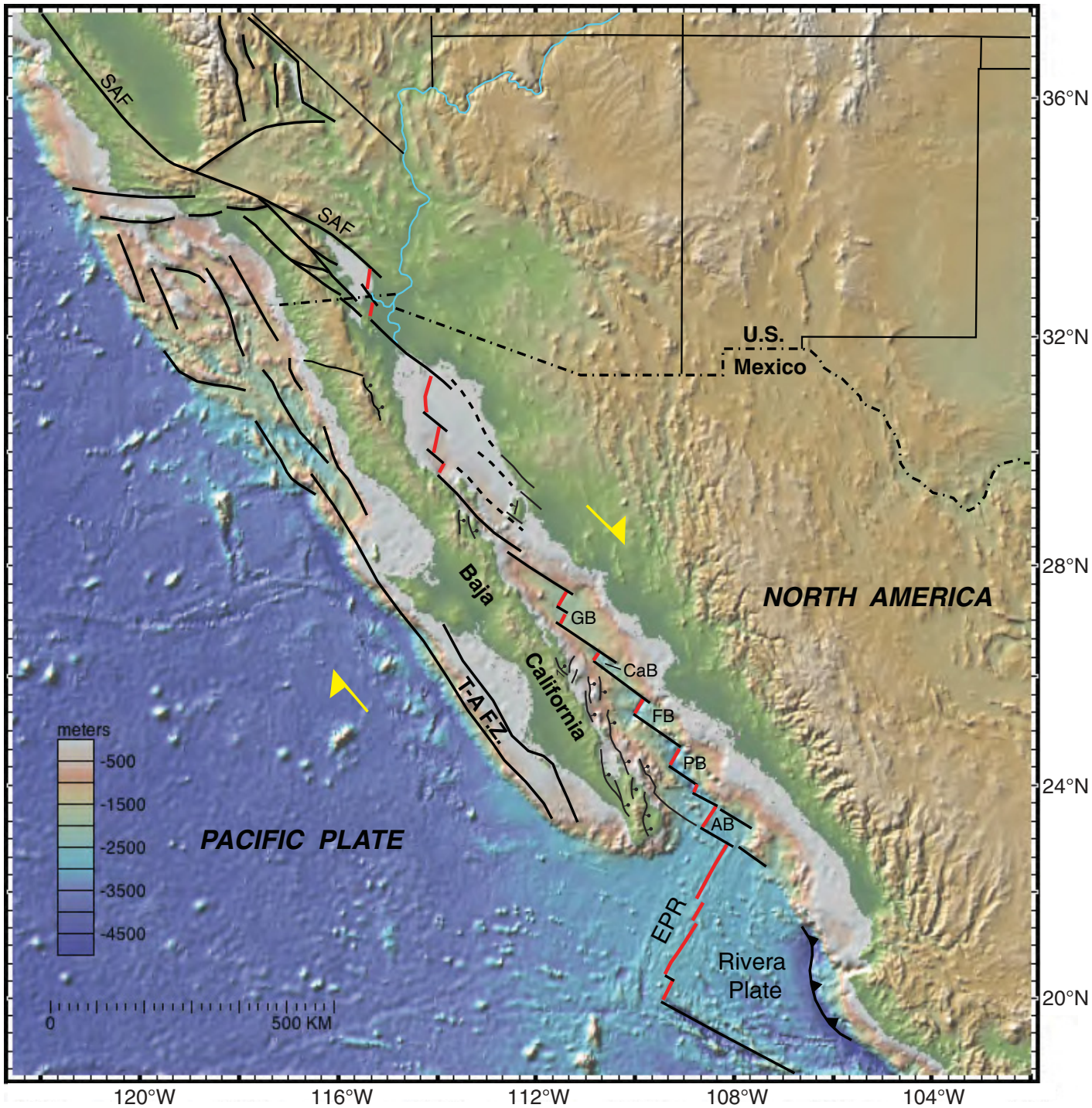

Figure 1. Map of topography, bathymetry, and faults in the Gulf of California and Salton Trough plate boundary. The gulf axis fault system comprises the transform faults and short spreading centers (red lines) along the center of the Gulf of California; the gulf margin fault system comprises the normal faults along the southeastern side of the Baja California peninsula; the borderland fault system is west of the peninsula. Abbreviations: AB—Alarcon basin; CaB—Carmen basin; EPR—East Pacific Rise; FB—Farallon basin; GB—Guaymas basin; PB—Pescadero basin; SAF—San Andreas fault; T-A F.Z.—Tosco-Abreojos fault zone.

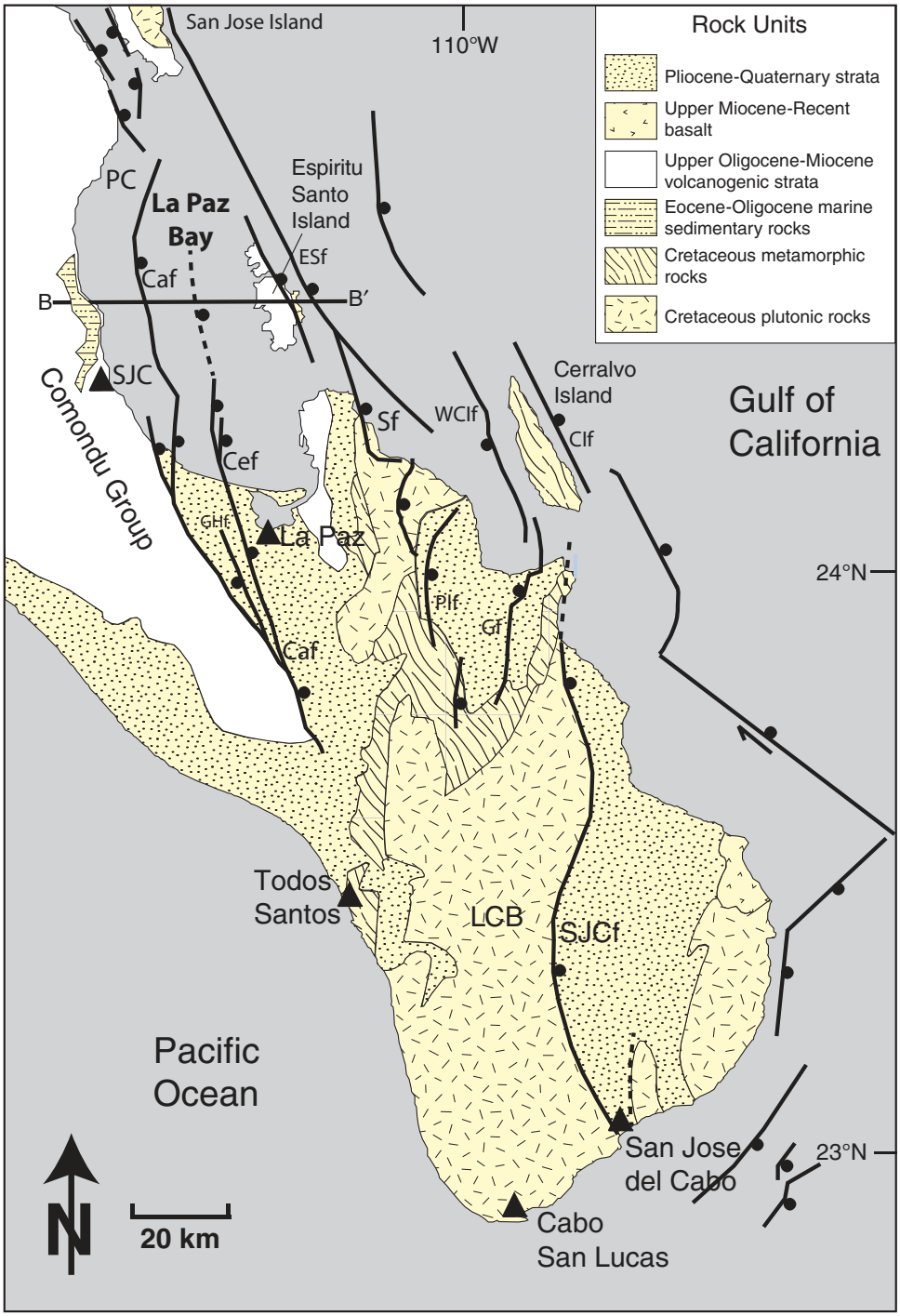

Figure 2. Geology onshore and the major faults of the La Paz to Los Cabos region. Abbreviations: Faults: Caf—Carrizal fault; Cef—Centenario fault; CIf—Cerralvo Island fault; ESf—Espiritu Santo fault; Gf—La Gata fault; GHf—Garambullo Hills fault; Plf—Los Planes fault; Sf—Saltito fault; WCIf—West Cerralvo Island fault. Cities (triangles): SJC—San Juan de la Costa. PC—Punta Coyote. Line B–B′ is the cross section line in Figure 12.

Mexico, and the geometry of the fault system, slip rate, earthquake recurrence rate, and possible slip per event refine our understanding of the hazard posed by these structures.

GEOLOGIC SETTING OF THE CARRIZAL FAULT

The plate boundary in the southern Gulf of California is composed of the main axial system of transform faults and spreading centers, and the stable Baja California microplate and the fault systems that border it (Fletcher and Munguía, 2000; Plattner et al., 2007; Busch et al., 2011). The three fault systems are referred to as the gulf-axis fault system, the gulf-margin fault system, and the borderland fault system (Fig. 1) (Fletcher and Munguía, 2000). The gulf-axis system defines the main Pacific–North American plate boundary, across which the majority of relative plate motion is accommodated through an array of en echelon right-stepping transform faults and ocean spreading centers (Fletcher and Munguía, 2000). The main spreading centers in the southern Gulf of California offshore of the present study area form small ocean deeps, and from south to north are the Alarcon basin and spreading center (or Alarcon Rise) and Pescadero and Farallon basins with their nascent spreading centers (Fig. 1).

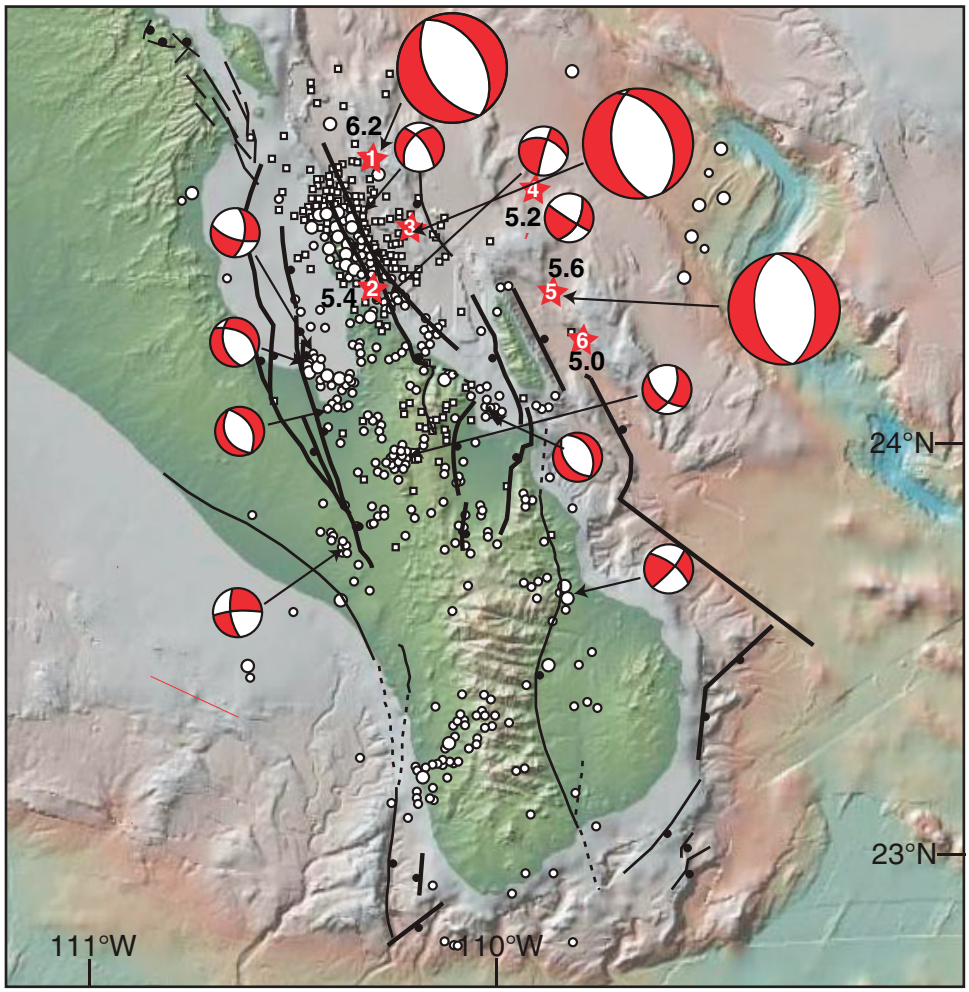

Figure 3. Microearthquakes (small white circles) (after Munguía et al., 2006) and larger earthquakes (red stars) since the 1960s in the La Paz region (after Molnar, 1973; Fletcher and Munguía, 2000). Large earthquakes: (1) Ms 6.2 on 6/30/95; (2) Ms 5.4 on 6/30/95; (3) Mb 4.1 on 6/30/95; (4) Mw 5.2 on 9/2/07; (5) Ms 5.6 on 4/4/69; (6) Ms 5.0 on 4/18/69.

The Alarcon spreading center has been active since 3.5–3 Ma (DeMets, 1995; Sutherland, 2006; Sutherland et al., 2012) with modern rates of spreading since 2.4 Ma (Sutherland, 2006). The borderland fault system lies offshore to the west of the Baja California peninsula and includes the active Tosco-Abreojos and San Benito fault zones (Dixon et al., 2000). The Baja California microplate bounds the gulf-margin fault system on the west and is moving at 47 mm/yr away from North America at the latitude of the southernmost portion of the peninsula (Plattner et al., 2007). The gulf-margin fault system consists partly of north to north-northwest–striking, predominantly east-dipping normal faults in the nearshore and onshore basins that accommodate a component of approximately east-west extension within an overall transtensional fault system along the margin of the plate boundary. Fletcher and Munguía (2000) pointed out that these normal faults are part of a pattern of regional strain partitioning.

Faults associated with the gulf-margin fault system cut across the southern tip of the Baja California peninsula and form a left-stepping array (Figs. 1 and 2). The primary faults of the gulf-margin fault system from the La Paz area southeast to San Jose del Cabo include the Carrizal, Espíritu Santo, San Juan de los Planes, La Gata–West Cerralvo, Cerralvo Island, and San José del Cabo faults (Fig. 2) (Fletcher and Munguía, 2000; Busch et al., 2011).

The Carrizal fault is a NW-striking, east-dipping normal fault that cuts near the base of the Gulf Escarpment onshore (Fig. 2) and defines the westernmost boundary of the gulf-margin system at the latitude of La Paz (Figs. 2 and 3). The fault extends ~70 km onshore south of La Paz Bay and continues ~50 km north across La Paz Bay to near Punta Coyote; the fault's northern projection or termination is uncertain (Fig. 2) (Drake, 2005; this study). This study focuses on a 28-km-long, ~3-km-wide strip along the northern part of the onshore Carrizal fault, the coastal belt of uplifted marine terraces on the west side of La Paz Bay, and on a series of underwater fault scarps in La Paz Bay revealed in a 2008 seismic CHIRP survey. The study area is bounded to the west by the Gulf Escarpment composed of rocks of the Comondú Group, parts of the forearc and volcanic arc before the Gulf of California formed, and older Tertiary marine strata (Hausback, 1984; Drake, 2005).

The onshore Carrizal fault exhibits broadly concave to the east geometric fault segments a few to 8–10 km long (Fig. 4). The offshore Carrizal fault may also be segmented, but is much less well characterized (Fig. 2). The shape of the coastline west of the offshore fault scarps also suggests ~10- to 20-km-long segments (Fig. 3). The boundaries between the onshore segments are characterized by abrupt changes in strike. At the hundreds of meters to km scale onshore, individual segments are straight rather than concave, and segments exhibit varying strikes with distinct bends between them (Fig. 4). This segment geometry is especially evident in the northernmost part of the onshore fault, where the fault cuts into resistant volcanic rocks of the Comondú Group, whereas to the south in the El Llano and Cuadridito segments the fault cuts partially lithified sandstones of the Comondú

Group and is not segmented at the few hundreds of meters scale.

Note that the earlier studies by our group (Busch et al., 2011; Coyan et al., 2013) show the Carrizal fault running offshore near the shoreline on the west side of La Paz Bay, while the newer CHIRP data of this study suggest that the main fault is ~15 km offshore from the west shoreline of La Paz Bay (Fig. 2). We cannot eliminate the possibility of a smaller fault splay (or splays) running near the shoreline, or an older fault that would not offset the seabed because we have no data from the nearshore belt. However, the CHIRP lines run close enough to the shoreline and at a shallow enough depth to suggest there are no active faults except those with minor (a couple meters or less) offset.

The Carrizal fault is interpreted to be older in the north offshore than in the south (Fig. 2). Topographic arching of footwall bedrock units, the presence of progressively older footwall rocks near the midsection of the arch, and offshore scarp heights all indicate that the fault is at a maximum long-term displacement offshore from 24°30 N to near San Juan de la Costa on the west side of La Paz Bay. A shallow basin along the onshore Carrizal fault confirms the interpretation that the oldest part of the fault is to the north (Busch et al., 2011).

METHODS

Onshore

Neotectonic analysis of the onshore Carrizal fault consisted of mapping of fault segments (compiled at 1:25,000 scale, Maloney, 2009) (Fig. 4B), paleoseismic investigations, and optically stimulated luminescence (OSL) geochronology of faulted sediment. Thirty fault-scarp–perpendicular topographic profiles were measured across the Carrizal fault (Fig. 4C). These fault scarp profiles were constructed to document the distribution of vertical offset along the fault.

We mapped the fault traces on georeferenced Mexican aerial photographs, topographic maps, and imagery available from Google Earth at 1:10,000 scale. In addition to documenting the discontinuous fault traces, we mapped the main Tertiary geologic units largely from aerial photography but emphasized the various Quaternary fluvial and alluvial fan units. Fault activity is defined by crosscutting relationships between the faults and the late Quaternary contacts.

Three fault-perpendicular exposures along the Carrizal fault were examined to assess the

Figure 4 (*Continued on following pages*). (A) Map of onshore faults, fault segments, fault trenches, gravity line A–A′ (from Busch et al., 2011), and cities (black circle and black text) on Google Earth image base map.

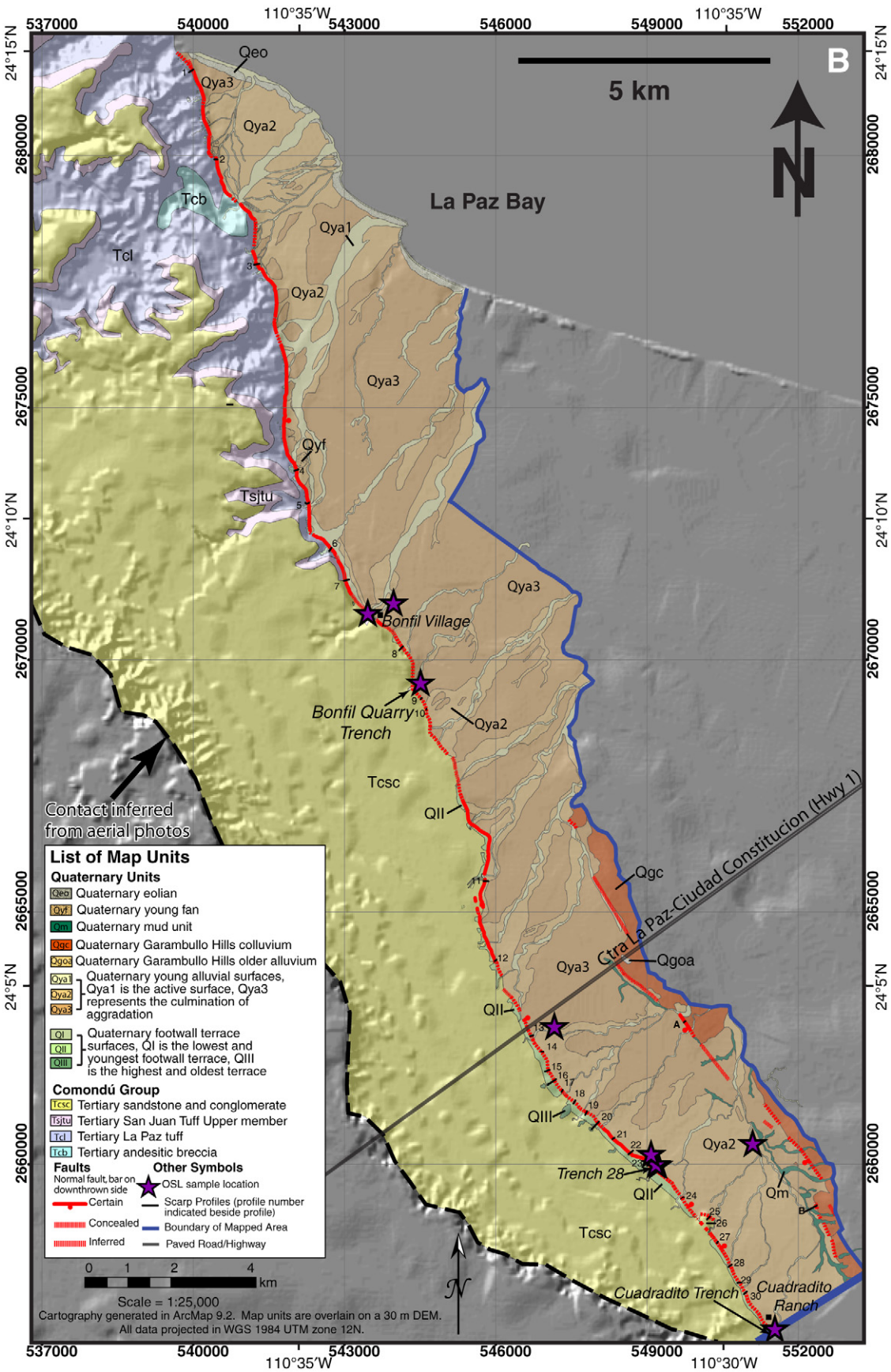

Figure 4 (*Continued*). (B) Geologic map of the onshore Carrizal fault (from Maloney, 2009).

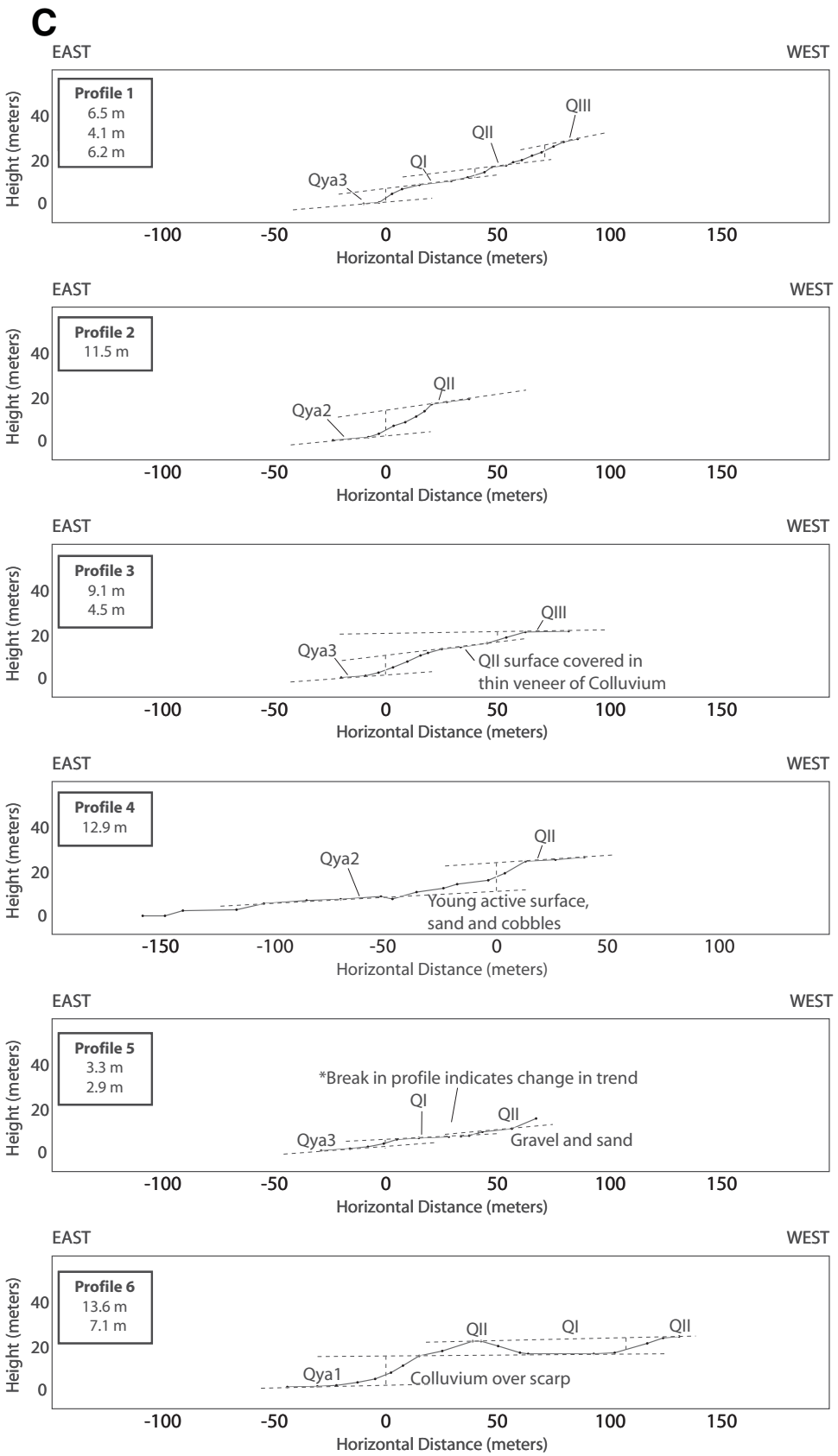

Figure 4 (*Continued*). (C) Thirty fault-perpendicular, fault scarp profiles presented from north to south (drawn east to west or facing south), highlight offset surfaces. The vertical offset measured between each footwall surface is given in the box with each Profile number. See locations on Figure 4B. Hand-leveled profiles illustrate offsets of late Quaternary correlative surfaces over ~100 m fault normal aperture.

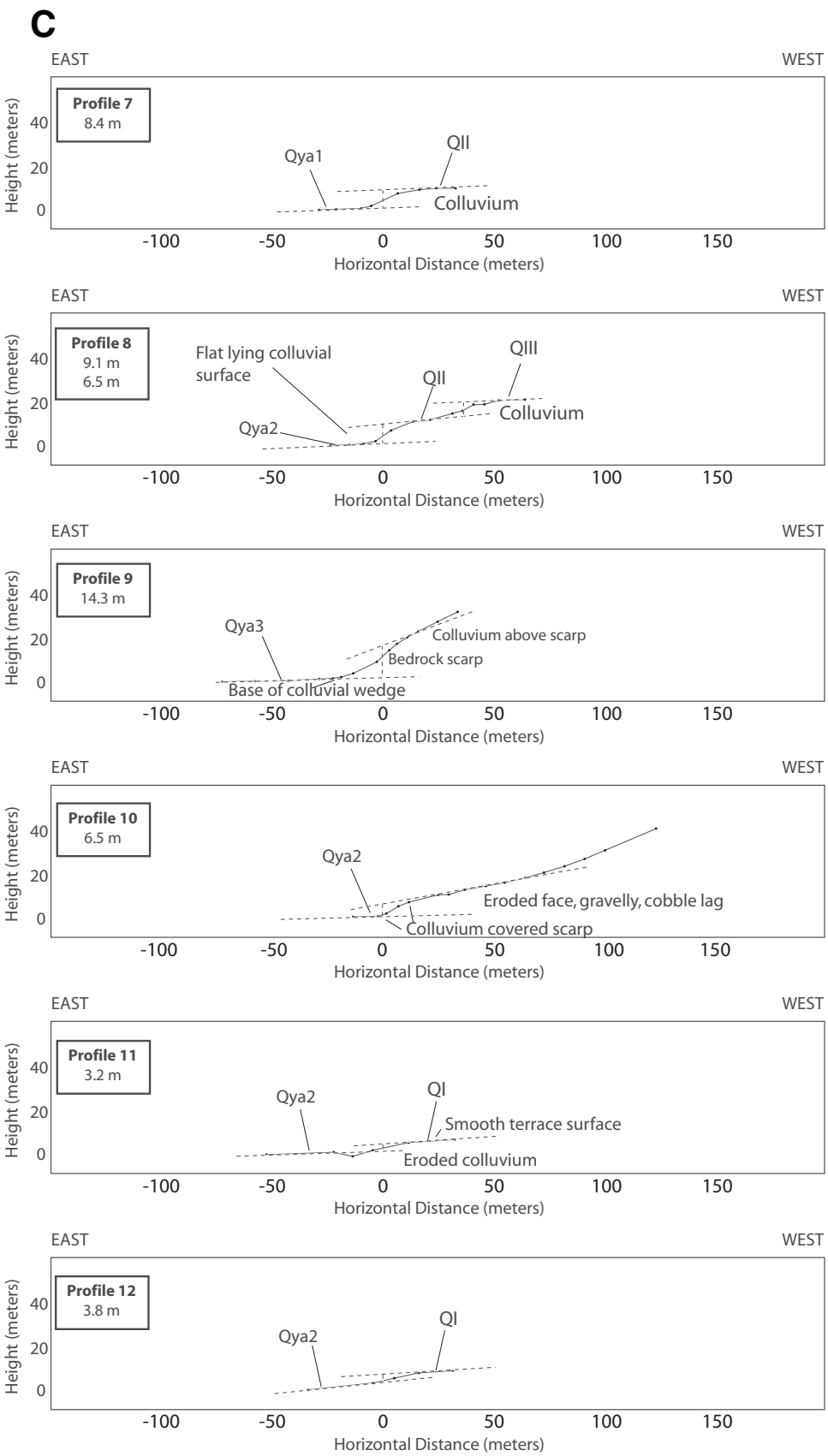

Figure 4 (*Continued*).

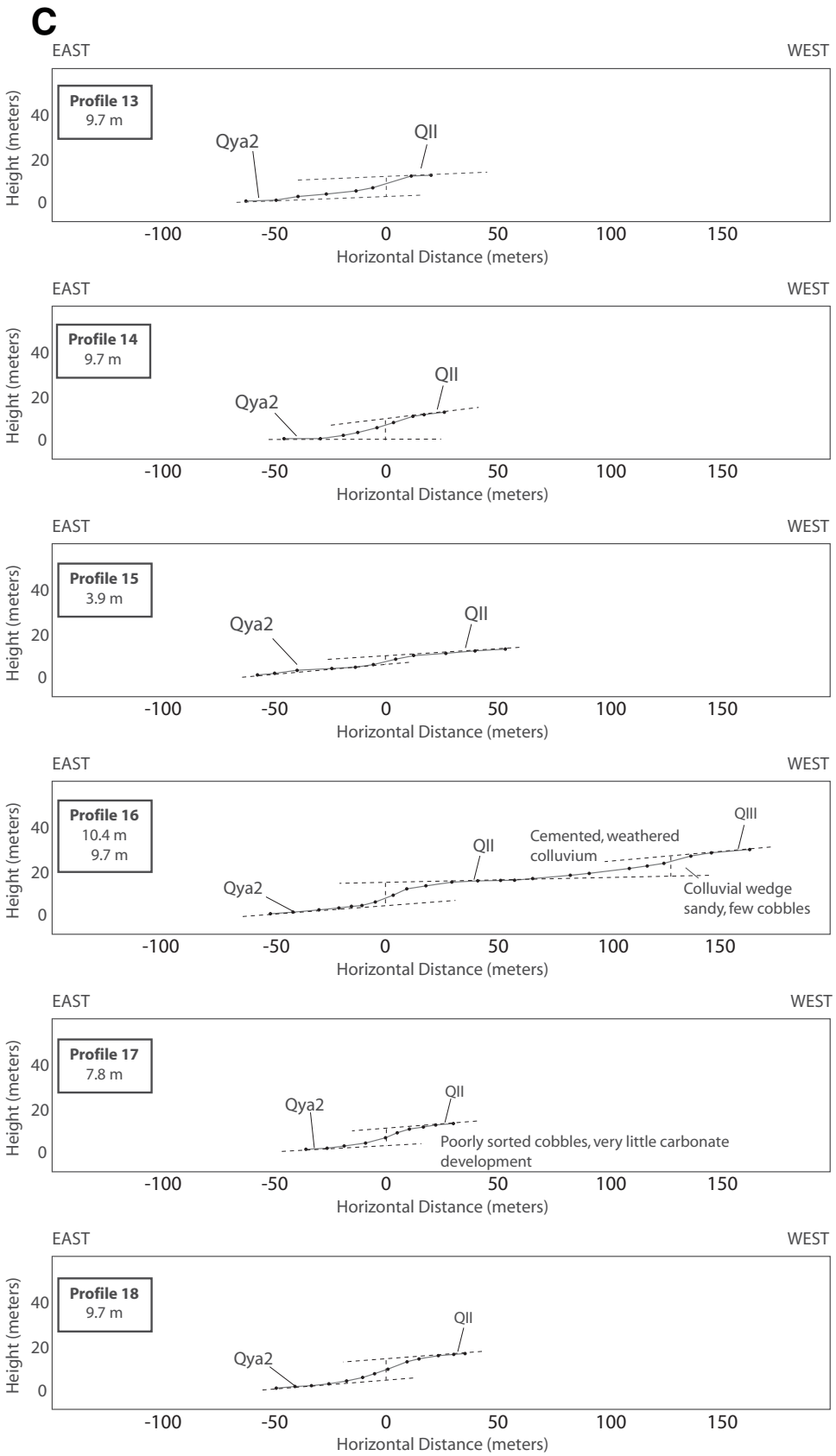

Figure 4 (*Continued*).

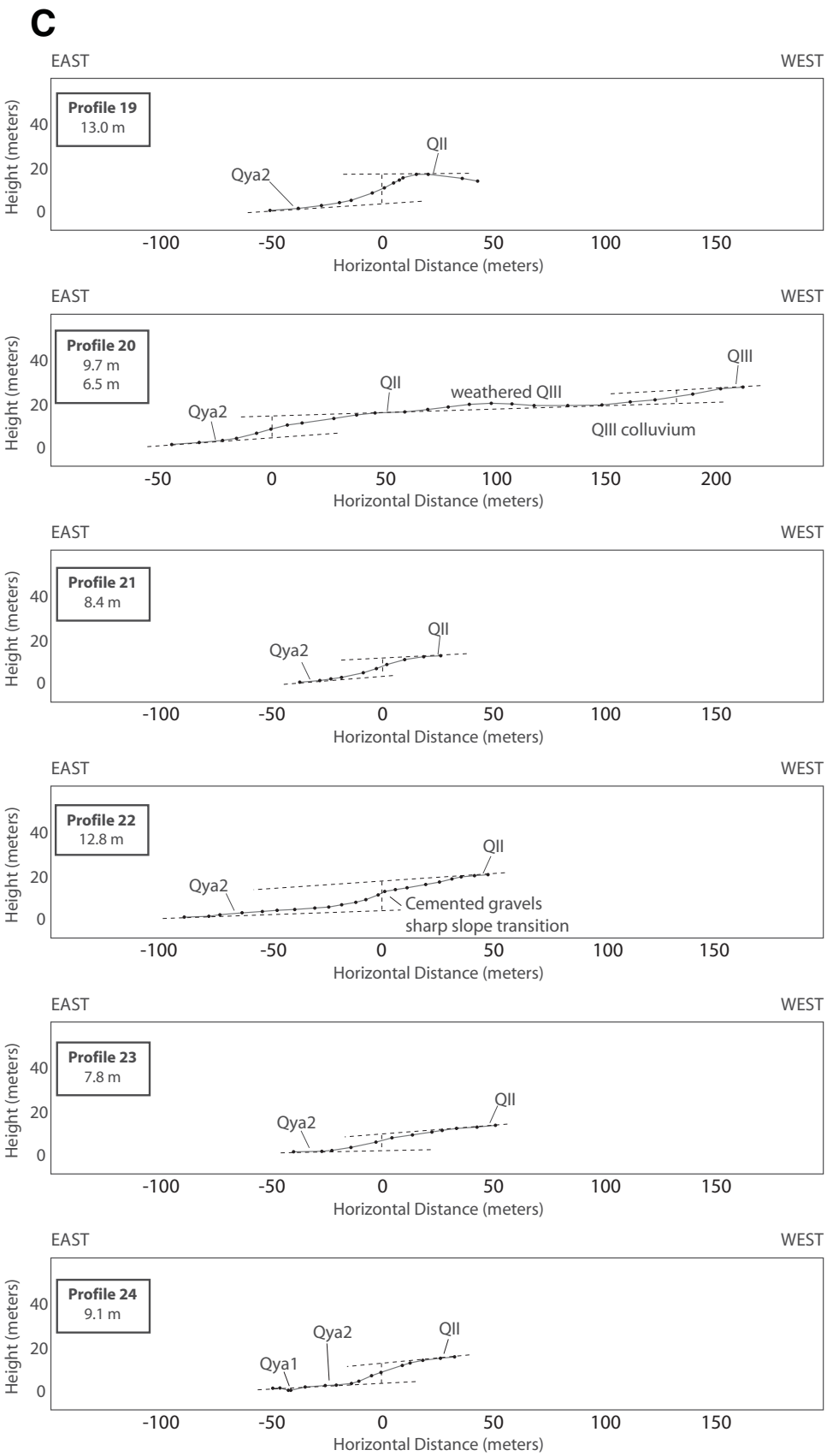

Figure 4 (*Continued*).

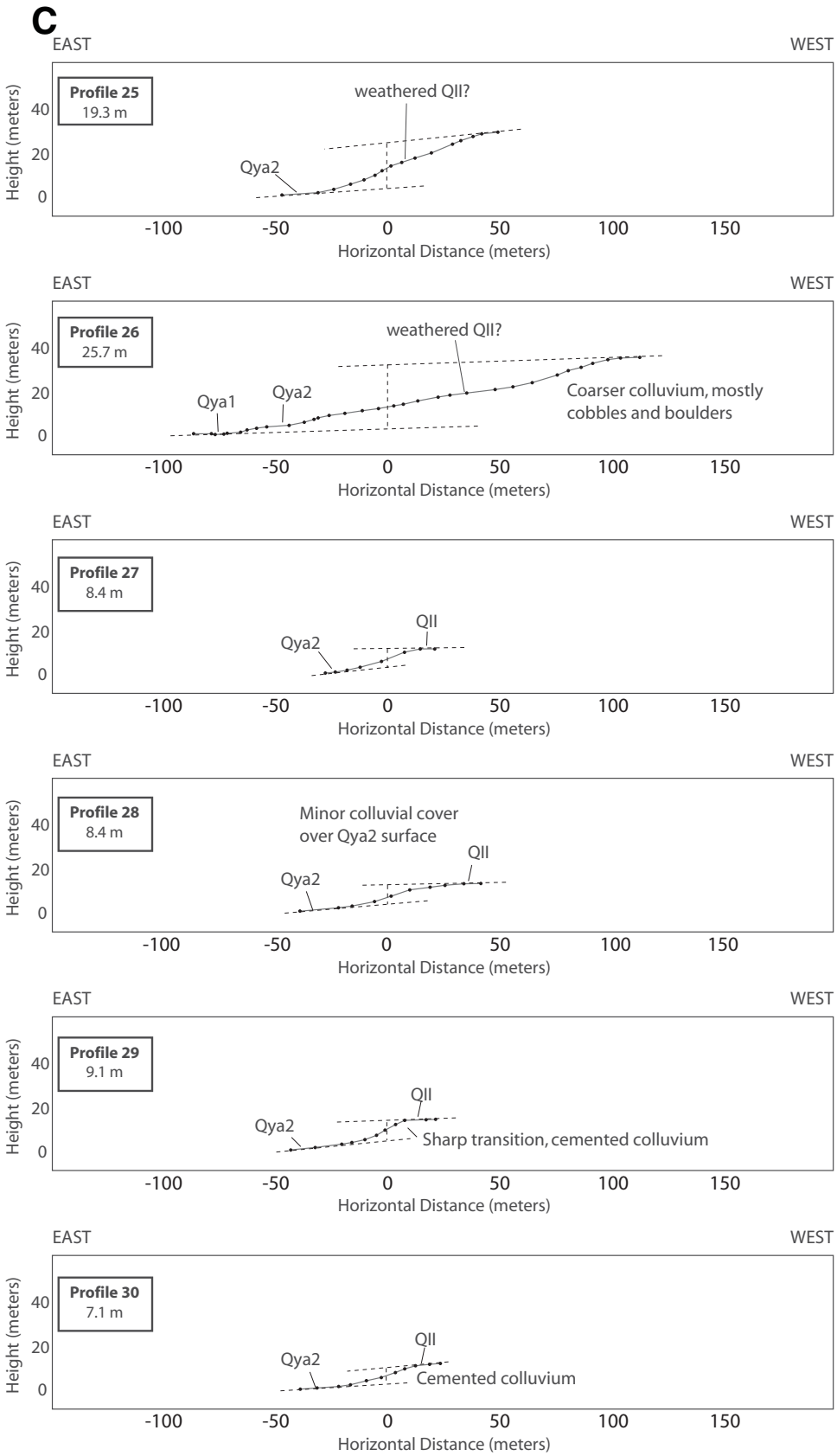

Figure 4 (*Continued*).

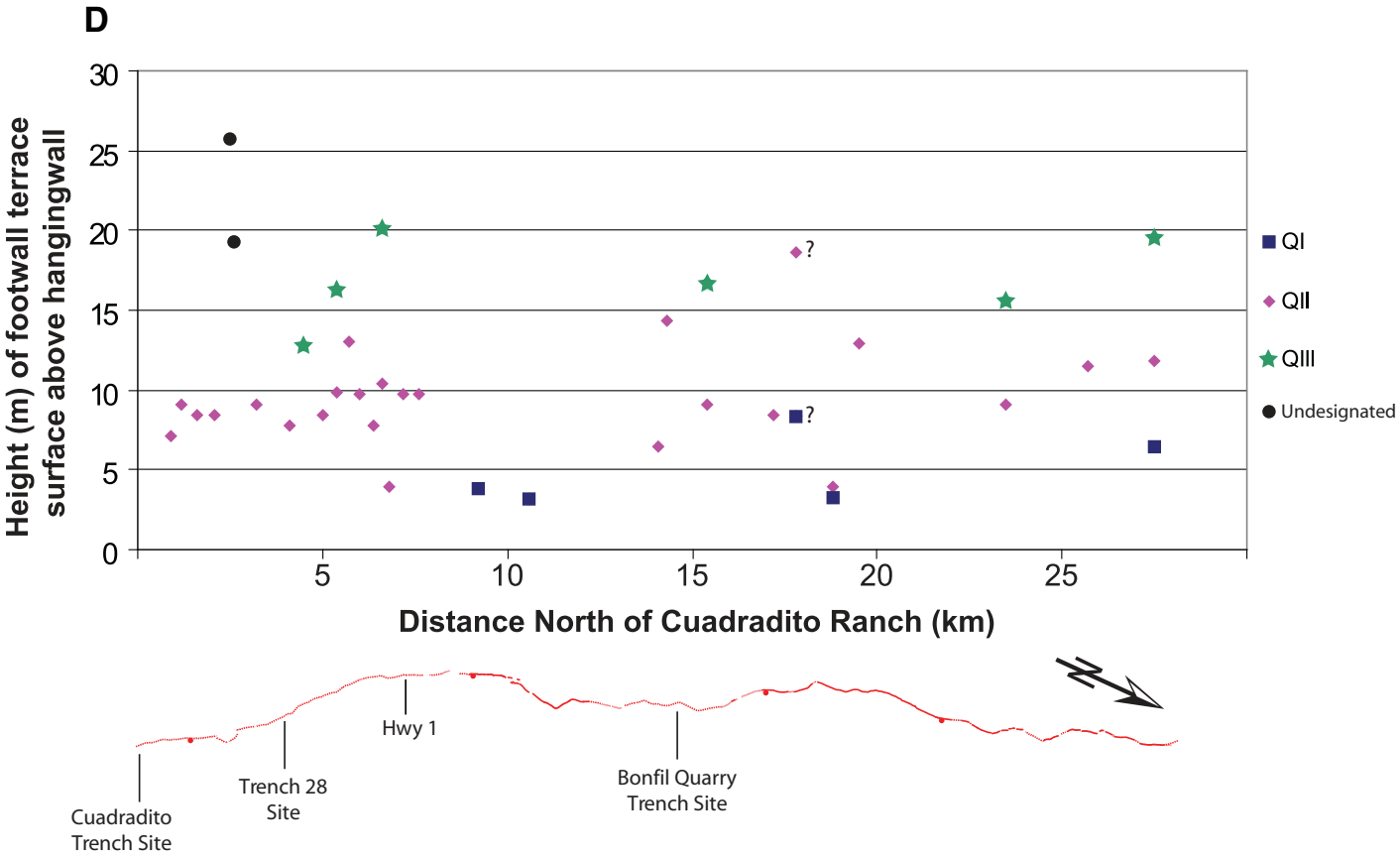

Figure 4 (*Continued*). (D) Graph of height of footwall terraces (from Fig. 4C) of onshore Carrizal fault versus distance north of Cuadradito Ranch.

millennial time-scale offset history along the fault. Trench 28 (17.5 m long by 2–5 m deep) was excavated ~23 km south of La Paz Bay (Figs. 4B and 5). A 20-m-long, 2- to 3-m-deep fault-perpendicular trench was excavated across an 8-m-high scarp of the Carrizal fault. The trench walls were photographed and hand logged at 1:20 scale (Fig. 5). About 1 km south of Rancho Bonfil, ~10 km north of Trench 28, and ~8 km south of La Paz Bay, a quarry road cut that exposes the fault zone was exploited for a second paleoseismic site (Fig. 4). It provides an excellent fault-perpendicular exposure of the fault zone with only modest onsite clearing. At this site, the exposed south wall was prepped and mapped at 1:20 scale (Fig. 6). A third trench site (Cuadradito Trench) was excavated ~4 km south of Trench 28 near the Cuadradito Ranch, but this trench did not reveal an interpretable earthquake record. The exposures were cleaned, gridded, photographed, and then the stratigraphy and fracturing documented at 1:25–1:50 scale. Charcoal was not present at any of the sites; therefore, several samples were collected for OSL analysis.

Optically stimulated luminescence (OSL) was utilized as the primary geochronological method for constraining uplift rates along the onshore Carrizal fault (as was done by Busch et al., 2011 and Coyan et al., 2013). A total of 16 samples were collected for analysis: five samples from Trench 28, two from the Bonfil quarry trench, two from the Cuadradito trench, and seven from fault-scarp proximal fluvial units (Tables 1, 2, and 3 and the Supplemental File[1]). The OSL dating technique provides an age estimate for the last time that sediments were exposed to light, which resets the luminescence signal. Luminescence dating of quartz grains was performed at the (Luminescence Laboratory at Utah State University in Logan, Utah). The methods used in the OSL dating are described in Maloney (2009) and in the Supplemental File (see footnote 1).

The optical ages generated for both fluvial map units and from the trench sites are summarized in Tables 1, 2, and 3. At Trench 28, Unit V was the only unit that contained sediments suitable for OSL dating. At the Bonfil quarry trench site, unit Hb was sampled for OSL analyses because it was the only exposed unit that contained material suitable for luminescence dating. The OSL ages were combined where appropriate using OxCal v. 3.10. OxCal uses a Markov chain Monte Carlo method to resample the age probabilities into a single probability given that they represented the same unit (Bronk Ramsey, 1995, 2001). The probability distributions from the OxCal calibration are reported in Maloney (2009), and the combined age results are indicated in Table 3. Both the 1σ and 2σ calibrated ages are shown in Table 3; for purposes of slip-rate calculations, the 2σ ages were used.

Offshore CHIRP and Marine Terrace Methods

To locate the Carrizal and related faults offshore, we conducted a marine seismic survey

[1]Supplemental File. Summary of all data and graphs of the new OSL ages reported in this paper. If you are viewing the PDF of this paper or reading it offline, please visit http://dx.doi.org/10.1130/GES00924.S1 or the full-text article on www.gsapubs.org to view the Supplemental File.

aboard a Mexican Navy vessel in August 2008, using the Scripps submeter-resolution Edgetech Subscan CHIRP system. The CHIRP profiler was operated with a 50 ms swept pulse of 0.7–3 kHz and provided decimeter vertical resolution and sub-bottom penetration >50 m. All data were digitally recorded in an internal EdgeTech JSF format (www.edgetech.com) (and later converted to SEG-Y format) with real-time global positioning system (GPS) navigation, providing location accuracy to within 5–10 m. Data were processed using SIOSEIS (http://sioseis.ucsd.edu) and imported to Kingdom Suite and IVS Fledermaus software packages for interpretation. A nominal water and sediment velocity of 1500 m/s was assumed for all depth and sediment thickness conversions.

To understand the rates of the offshore Carrizal faulting, we studied a series of uplifted marine terraces well exposed along the western side of La Paz Bay. The terraces were mapped in detail and described, and the height of the terraces was measured above sea level. Ages of Quaternary marine terraces were estimated by analyzing the extent of racemization in amino acids preserved within carbonate fossils of the mollusk genus Chione following the methods of Wehmiller and Miller (2000). Amino acid racemization ratios were corroborated by comparison to U-Th ages reported for marine terraces in the northern part of our study area (DeDiego-Forbis et al., 2004), and then these ages were used with the terrace heights to determine surface uplift rates and inferred offset. Racemization is a first-order reversible reaction with a rapid initial rate followed by a significantly decreasing rate (Kennedy et al., 1982; Wehmiller and Miller, 2000). Apparent parabolic kinetics converts the nonlinear rate into a linear rate and provides a means of calculating ages of fossils from similar climatic regions. The apparent parabolic kinetics model is based on the empirical observation that the rate of racemization in natural material conforms to a square-root function, $D/L = kt^{0.5}$ (Mitterer and Kriausakul, 1989). This relationship yields the equation, $t = [(D/L)_s/mc]^2$, where t is the calculated age of the unknown sample in years, $(D/L)_s$ is D/L in the sample of unknown age, and mc is the slope ($(D/L)/t^{1/2}$) obtained from the calibration sample.

Amino acid racemization analysis from fossils of the same genus will yield the same value, if they have similar thermal and burial histories. The rate of racemization is controlled by the temperature experienced by the fossil since death of the animal, and therefore, temperature increases with proximity to equatorial latitudes and with burial depths <1 m (Kennedy et al., 1982; Wehmiller and Miller, 2000). Diurnal temperatures are damped out in the upper few

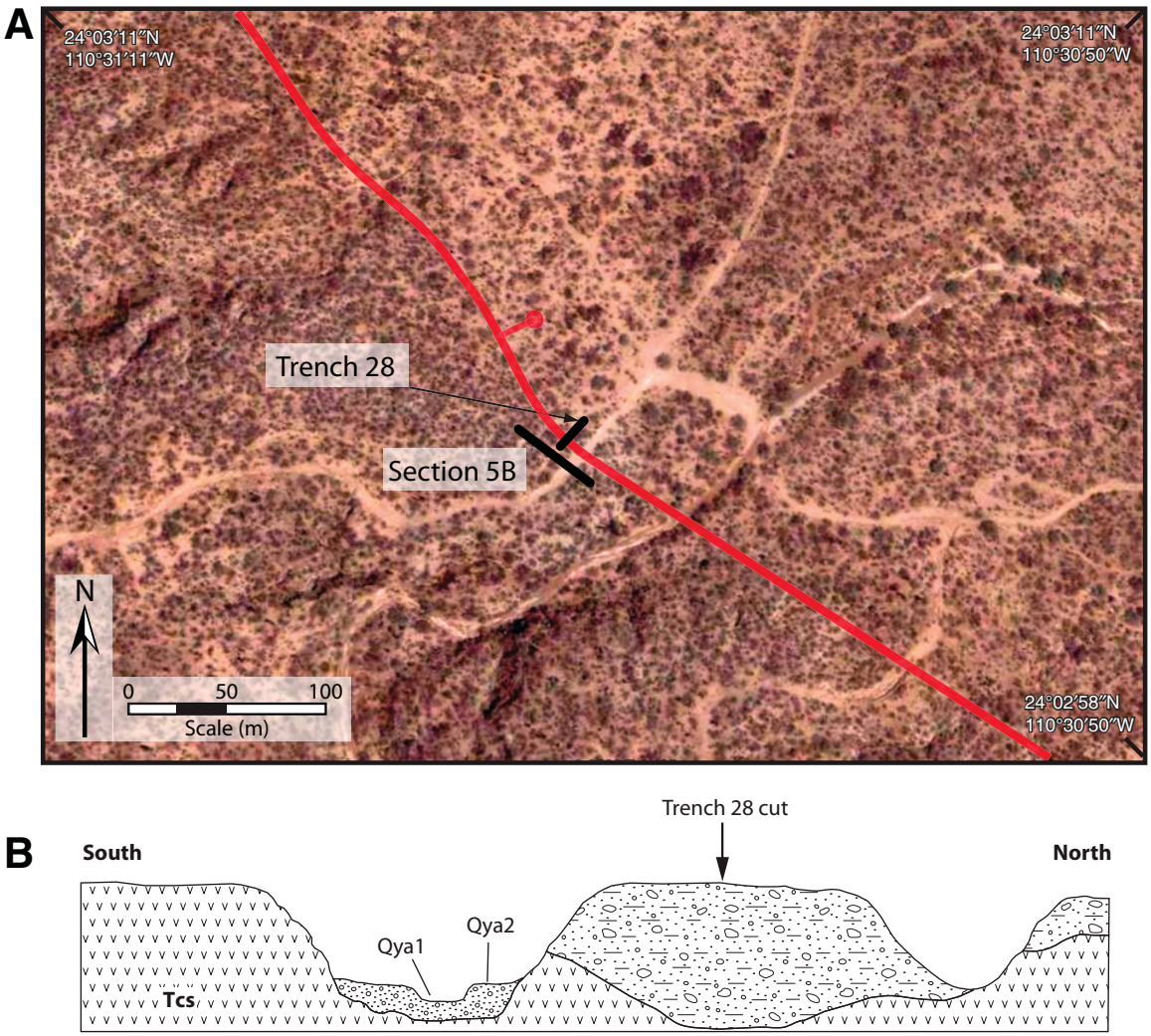

Figure 5 (*Continued on following page*). (A) Trench 28 site on Google Earth image illustrating piedmont setting. (B) Cross section of local geomorphic features near Trench 28.

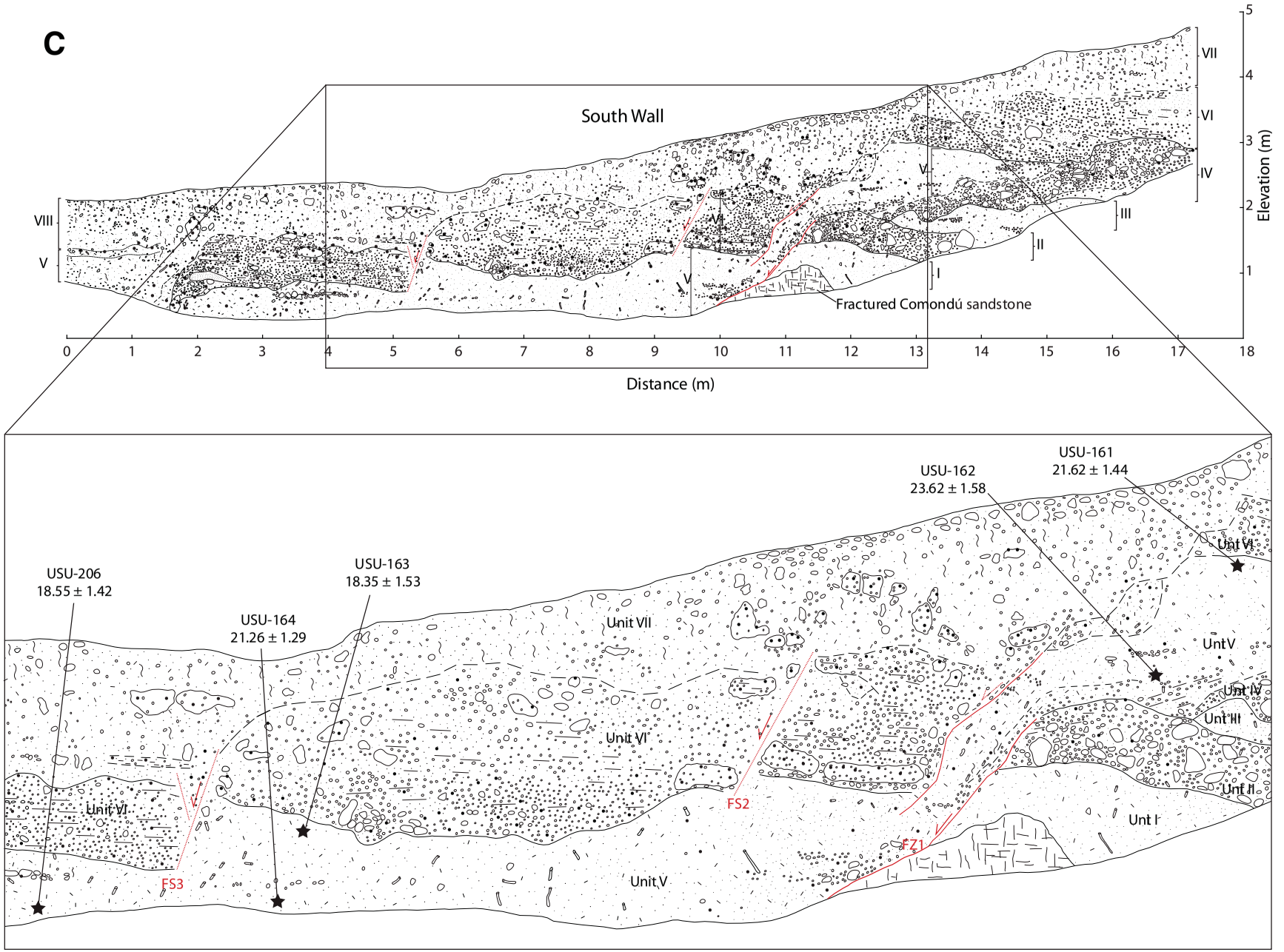

Figure 5 (*Continued*). (C) Trench 28 paleoseismic log and enlargement of Trench 28 south wall fault zone 1, and fault strands 2 and 3. Fault strands probably continue down dip into unit V but could be traced because of its massive character with no obvious fabric. See Figure 7 for a reconstruction of the offset history inferred from this record. Optically stimulated luminescence (OSL) ages for unit V are indicated.

centimeters below ground surface, but the seasonal oscillation can penetrate at least 1 m into the subsurface (Wehmiller and Miller, 2000). To minimize the effect of seasonal and diurnal temperature fluctuations, samples were collected from similar, contiguous deposits with depths >1 m, preferably in arroyo cuts. All 12 samples were prepared according to the procedures of Kaufman and Manley (1998) and Wehmiller and Miller (2000) for reverse-phase and ion-exchange, high-performance liquid chromatography analysis, respectively, and processed in the Northern Arizona University Amino Acid Geochronology Laboratory.

RESULTS—ONSHORE CARRIZAL FAULT

Map Units

In the study area, the southern end of the Sierra de la Giganta and its southern extension forms the mountain range and rift escarpment immediately west of the Carrizal fault. The bedrock geology of the coast is built in ascending order of the upper Oligocene San Gregorio Formation, the lower Miocene Isidro Formation, and the lower to middle Miocene terrestrial Comondú Group (Hausback, 1984). The marine San Gregorio and Isidro formations were later described and renamed the El Cien Formation (Gidde, 1992; Fischer et al., 1995), and those strata are exposed near San Juan de la Costa on the west side of La Paz Bay (Fig. 2). The Comondú Group forms the bedrock in the footwall of the Carrizal fault south of, and more than 20 km north of, San Juan de la Costa (Fig. 2).

The Comondú Group is a sequence of Oligocene–Miocene arc-derived clastic rocks and silicic to intermediate volcanic and volcaniclastic rocks (Hausback, 1984; Drake, 2005). Regionally, the Comondú Group consists of a lower clastic unit with common tuffs and local volcanic breccias in the La Paz area (Hausback, 1984; Drake, 2005), a middle unit of mainly volcanic breccias, and an upper unit of andesitic lavas and breccias mainly exposed north of La Paz Bay. The footwall of the Carrizal fault onshore is mainly a conglomerate and sandstone unit that lies above the prominent San Juan Tuff.

Within the Quaternary units, three footwall terrace surfaces (QI, QII, and QIII) and three hanging-wall fluvial surfaces and underlying units (Qya_1, Qya_2, and Qya_3) were identified. Note that these footwall and hanging-wall units probably correlate (corresponding Roman and Arabic numerals) based on relative height, soil development, and degradation of original surficial features; but as a conservative approach, we have delineated them separately. Additional map units include volcanic and volcaniclastic rocks of the Comondú Group in the footwall and eolian beach deposits on the hanging wall.

The hanging wall of the onshore Carrizal fault contains a Quaternary basin that varies in width from 1.5 to 4.5 km from south to north (Fig. 4B). The basin is bounded to the east by the Garambullo Hills, a horst composed of uplifted Quaternary alluvium between the Garamullo Hills and Centenario faults (Figs. 2 and 4A). Map units associated with the Garambullo Hills fault (Fig. 4A) include one additional hanging-wall unit (Qm) and two footwall units (Qc and Qgoa) (Fig. 4B). The basin forms a broad, gently north-northwest–sloping alluvial floodplain that drains into La Paz Bay. South of Baja Highway 1, a large active drainage cuts across the Garambullo Hills and drains into La Paz Bay northwest of the village of Centenario (Fig. 4A). Three incised alluvial surfaces and their deposits were identified in the basin deposits.

At least three, and up to five, levels of Quaternary geomorphic surfaces (QI, QII, and QIII) are present on the footwall of the onshore Carrizal fault. These footwall surfaces apparently represent planed-off piedmont surfaces that were preserved as they were uplifted out of the zone of active fluvial processes. The footwall terraces are less well defined toward the south as the footwall transitions from bedrock dominated to a combination of bedrock and alluvial dominated. In the north, these footwall surfaces are correlated at similar elevations to the four uplifted marine terraces mapped along the west side of La Paz Bay and described below.

Fault Scarp Profiles

The 30 fault scarp profiles quantify the scarp characteristics and allow first-order conclusions. In general, the footwall of the northern half of the onshore Carrizal fault is characterized by steeper topography. Toward the south, the footwall topography is less pronounced, and the surface expression of the fault is characterized by a simple, single-step fault scarp morphology. The height of the fault scarp ranges from ~3 to 26 m (Figs. 4C and 4D). The profiles suggest that the footwall of the Carrizal fault displays more topographic variability along northern segments where more footwall surfaces (QI, QII, and QIII) are preserved. In the far south,

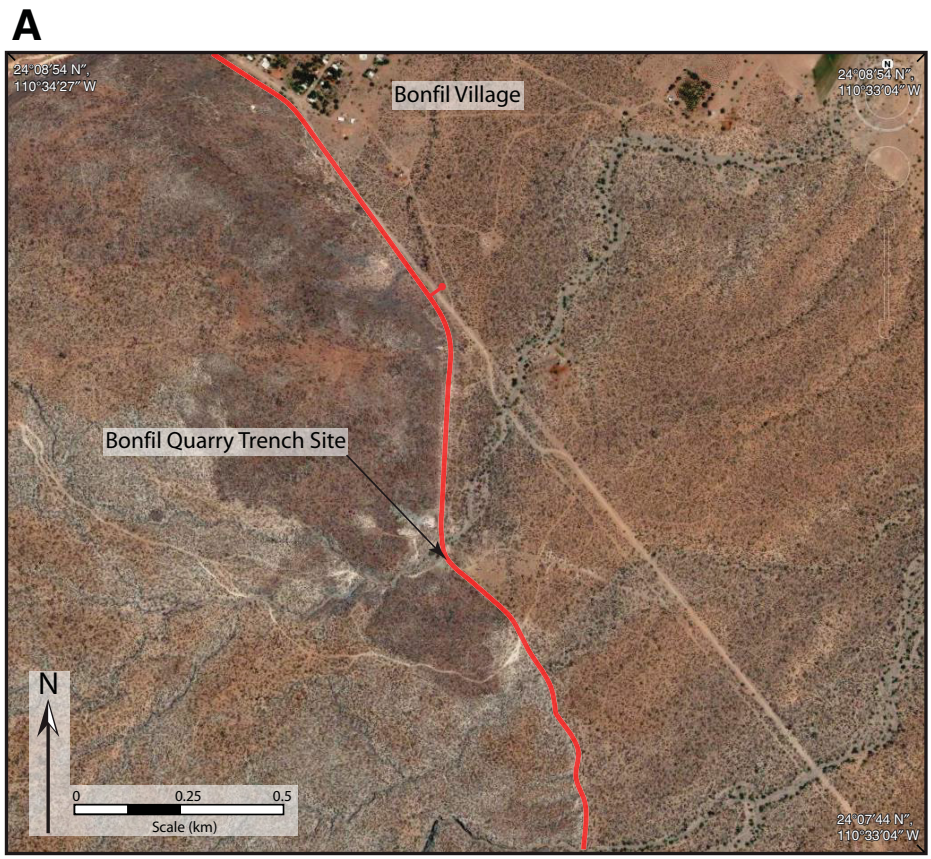

Figure 6 (*Continued on following page*). (A) Bonfil quarry trench site Google Earth image base map.

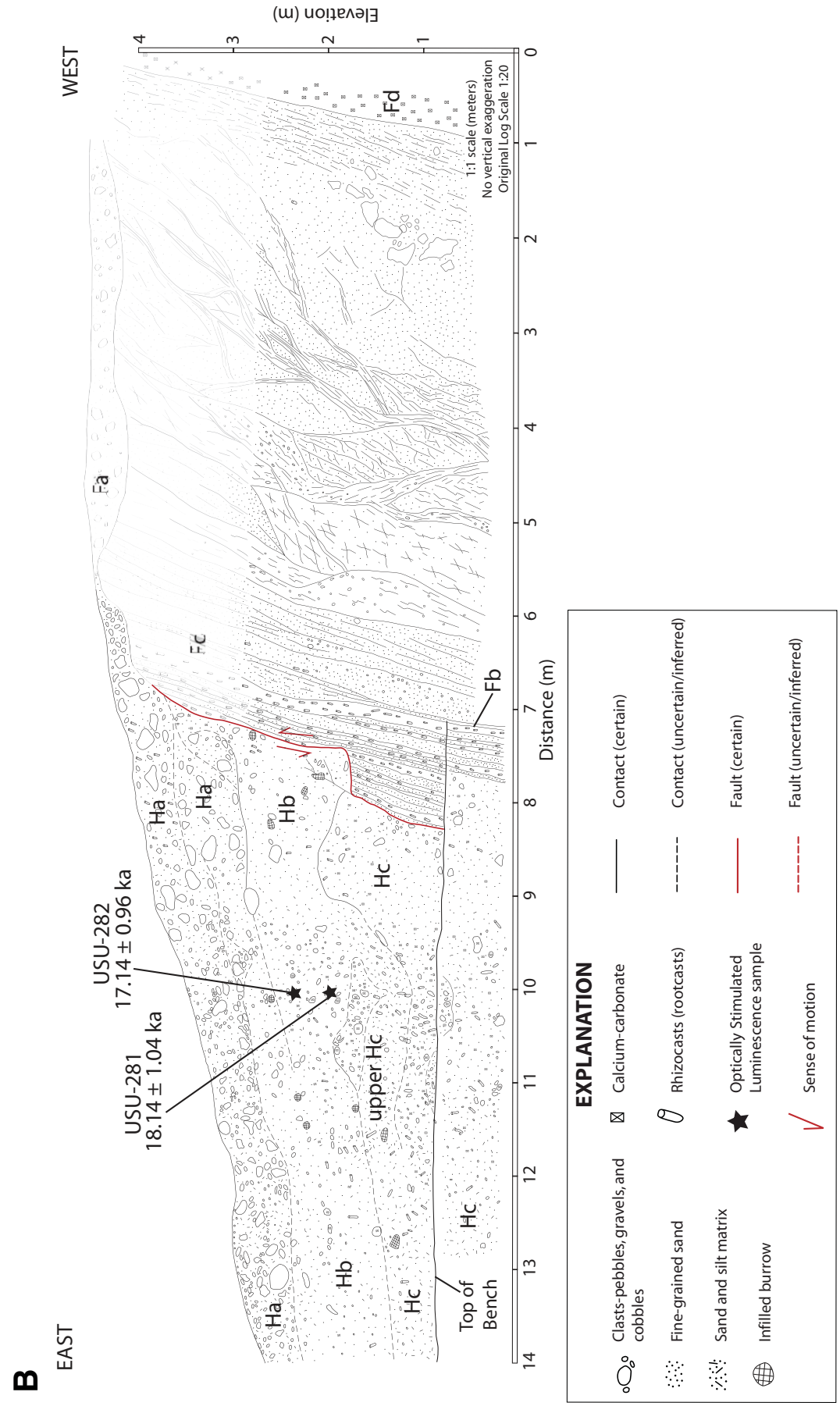

Figure 6 (*Continued*). (B) Bonfil quarry paleoseismic log. Lighter areas were drawn from photographs. Alluvium is faulted down against heavily sheared Comondú Group. See Figure 8 for a reconstruction of the offset history inferred from this record. Optically stimulated luminescence ages for unit Hb are indicated.

TABLE 1. LUMINESCENCE DATA FROM MAPPED FLUVIAL SURFACES

Sample no.	Field ID	Map unit	Depth (m)	Grain size (μm)	H_2O (%)	Dose rate (grays/ky)	Equivalent dose (grays)	OSL age (ka)
USU-167	SJM-040207-8A	Qya_2	0.96	75–125	1.1	3.02 ± 0.12	3.88 ± 1.69	1.28 ± 0.13*
USU-168	SJM-011707-5A	Qya_3	3.0	75–125	0.7	2.98 ± 0.12	22.27 ± 6.13	7.42 ± 0.57*
USU-173	SJM-011607-2D	Qya_2	0.8	75–125	1.0	3.52 ± 0.16	4.18 ± 1.71	1.19 ± 0.12
USU-174	SJM-011707-6A	Qya_3	1.3	75–125	0.8	2.97 ± 0.13	30.88 ± 6.59	10.39 ± 0.71*
USU-175	SJM-011607-4A	Qya_2	1.1	75–125	1.0	3.25 ± 0.15	11.57 ± 2.77	3.56 ± 0.87*
USU-204	SJM-011507-1A	QII	1.0	75–180	1.0	3.34 ± 0.15	45.83 ± 19.02	13.71 ± 1.40*
USU-205	SJM-011607-3A	Qya_2	0.85	75–125	1.0	3.64 ± 0.16	21.92 ± 8.06	6.02 ± 0.56†

Note: OSL—Optically Stimulated Luminescence.
*Sample analyzed using a double SAR protocol to remove feldspar signal (following Olley et al., 2004).
†Sample analyzed using a three second, 1% diode short shine to remove ultrafast signal (following Goble and Rittenour, 2006).

TABLE 2. LUMINESCENCE DATA FROM THE TRENCH 28, BONFIL QUARRY, AND CUADRADITO TRENCH SITES

Sample no.	Field ID	Trench site	Trench unit	Depth (m)	Grain size (μm)	H_2O (%)	Dose rate (grays/ky)	Equivalent dose (grays)	OSL age (ka)
USU-161	SJM-040807-9A	Trench 28	V	1.0	75–125	0.9	3.10 ± 0.13	67.02 ± 15.70	21.62 ± 1.44
USU-162	SJM-040807-9C	Trench 28	V	1.3	75–150	0.8	3.52 ± 0.15	83.16 ± 19.26	23.62 ± 1.58
USU-163	SJM-040807-10A	Trench 28	V	1.4	75–125	1.1	3.25 ± 0.14	59.64 ± 18.05	18.35 ± 1.53
USU-164	SJM-040807-10B	Trench 28	V	1.8	75–125	0.9	3.20 ± 0.14	68.01 ± 11.27	21.26 ± 1.29*
USU-206	SJM-040807-11A	Trench 28	V	1.3	75–125	1.1	3.34 ± 0.14	61.95 ± 17.15	18.5 ± 1.42
USU-165	AUS-02	Cuadradito	Qya_2	1.1	75–150	1.4	3.15 ± 0.13	11.71 ± 4.15	3.72 ± 0.34*
USU-166	AUS-03	Cuadradito	Qya_2	0.7	75–125	1.4	3.02 ± 0.12	6.33 ± 2.24	2.10 ± 0.18*
USU-281	Bonfil-A	Bonfil	Hb	1.5	75–180	2.3	2.84 ± 0.12	51.46 ± 7.55	18.14 ± 1.04*
USU-282	Bonfil-B	Bonfil	Hb	1.3	75–180	2.6	2.83 ± 0.12	48.55 ± 6.34	17.14 ± 0.96*

Note: OSL—Optically Stimulated Luminescence.
*Sample analyzed using a double SAR protocol to remove feldspar signal (following Olley et al., 2004).

TABLE 3. SUMMARY OF WEIGHTED MEAN AGES

Sedimentary unit	OSL age (ka)	Average age (ka)	Weighted average (ka)
Qya_2	1.19 ± 0.12 1.28 ± 0.13 2.10 ± 0.18 3.56 ± 0.87 3.72 ± 0.34 6.02 ± 0.56	2.98 ± 1.84	1.62 ± 76
Qya_3	7.42 ± 0.57 10.39 ± 0.71	8.91 ± 2.1	8.58 ± 0.44
Trench 28 Unit V	18.35 ± 1.53 18.5 ± 1.42 21.26 ± 1.29 21.62 ± 1.44 23.62 ± 1.58	20.67 ± 2.24	20.64 ± 0.65
Bonfil Trench Unit Hb	17.14 ± 0.96 18.14 ± 1.04	17.64 ± 0.71	17.6 ± 0.71

Note: OSL—Optically Stimulated Luminescence.

near Cuadradito Ranch (Fig. 4B), the fault scarp is not as high, and the number of Quaternary surfaces preserved on the footwall decreases. Approximately 3 km north of Cuadradito Ranch, there is a sharp bend in the surface trace of the El Carrizal fault (Fig. 4D) and the escarpment reaches a maximum height of ~26 m. Between Cuadradito Ranch and km 10 north of it, QI is absent and QIII is preserved as isolated remnants recessed several meters into the footwall (Fig. 4C, profiles 16 and 20). From the Bonfil quarry to the north, the escarpment reaches a maximum height of ~20 m on the QIII surface. The QII unit is predominant along the entire onshore fault and averages ~10 m above the hanging wall (Fig. 4D).

Paleoseismic Trenches

We excavated three trenches along the Carrizal fault (Figs. 4–6). The Cuadradito site was cut across young alluvial fan deposits within which we could find no evidence of fault offset. Two sites where the Carrizal fault was exposed and logged showed evidence of past earthquakes: Trench 28 and Bonfil. At Trench 28, the excavation was across alluvial deposits (Fig. 5), while the Bonfil quarry excavation, which we cleaned and expanded, showed Quaternary alluvium on the hanging wall juxtaposed against faulted bedrock in the footwall (Fig. 6).

Trench 28 revealed one paleoearthquake and was excavated ~70 m north of an active arroyo and a few meters south of a small gully (Figs. 5A and 5B). The entire sedimentary sequence preserved at the Trench 28 site is interpreted to be the remnants of a paleochannel, which facilitated the preservation of at least one earthquake event. The oldest sedimentary unit at this site is a small block of fractured sandstone of the Comondú Group on the footwall (Figs. 5C and 7). Overlying this block of sandstone is Unit I, which is interpreted to be the weathered remnants of the sandstone. Root casts in Unit I indicate some landscape stability after Unit I deposition. After erosion and stripping of the Comondú sandstone, the alluvial channel migrated to the present location of Trench 28 and deposited the sequence of fine-grained fluvial sands, gravels, and cobbles that comprise units II–V (Fig. 5C).

At the Trench 28 site, the principal fault zone (FZ1 in Fig. 5) is expressed by a 0.5-m-thick, wedge-shaped deposit that consists of silty sand from unit V with rotated blocks of carbonate-cemented gravels eroded from unit VI (Fig. 5). The principal fault zone dips ~60° east and offsets units V and VI. Two east-dipping subsidiary fault strands, FS2 and FS3, offset unit VI, but unlike the principal fault zone, do not have

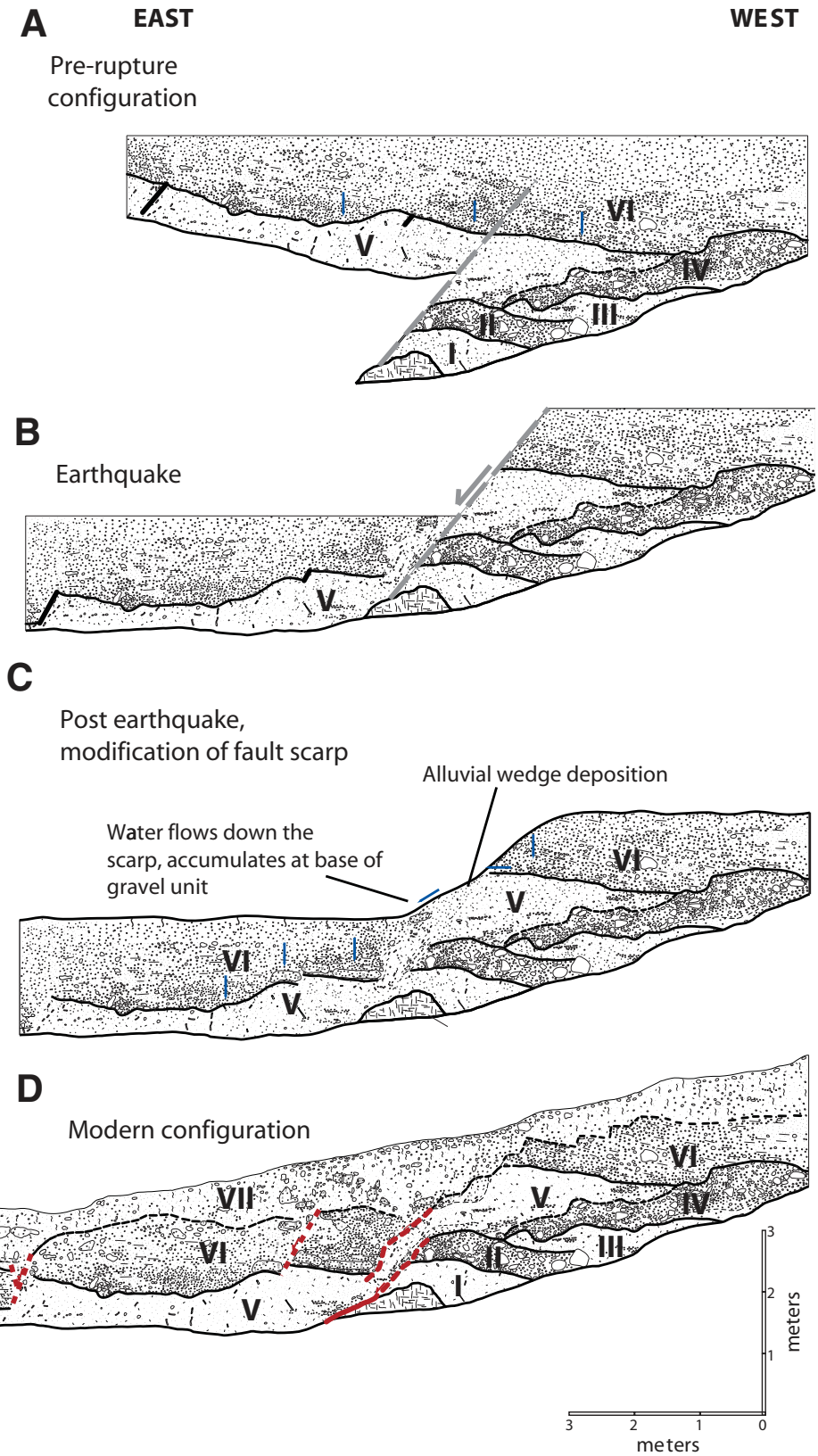

Figure 7. Sequence of events from an interpretation of the Trench 28 paleoseismic log. See text for discussion.

well-developed shear zones within unit V (Fig. 5). None of the well-defined faults in the trench logs have a corresponding sharp surface expression. Correlation of the base of unit V across the documented fault zone yielded a total stratigraphic vertical separation of ~2 m.

Five OSL ages were obtained from unit V: two from the footwall (21.62 ± 1.44 ka and 23.62 ± 1.58 ka) and three from the hanging wall (18.35 ± 1.53 ka, 21.26 ± 1.29 ka, and 18.55 ± 1.42 ka), with a mean age of 20.64 ± 0.65 ka (Tables 2 and 3 and Fig. 5C). These ages date the termination of unit V deposition and the onset of unit VI deposition. However, the transition from unit V to unit VI does not represent a conformable sequence, that is, there is no evidence observed within unit V to suggest a fining upward or coarsening upward transition that would indicate a gradual change in flow regime. Unit V was likely deposited during a single, rapid flooding event between ca. 18 and 23 ka. Unit V pinches out toward the west, which suggests that it may have been deposited in a scarp-parallel direction. Unit VI represents a fluvial bar deposit that scoured into unit V. Unit VI contains a faint subhorizontal fabric on the hanging wall, whereas on the footwall the fabric dips slightly westward; this difference in dip may have resulted from the most recent earthquake (Figs. 5C and 8). The base of unit VI on the hanging wall is heavily cemented, whereas unit VI on the footwall is only moderately cemented; this difference in cementation may be the result of subsurface water ponding at the more impermeable fault zone (Fig 5).

Only one faulting event was revealed with confidence at Trench 28 (Fig. 7). The most recent earthquake at Trench 28 apparently occurred after the deposition of unit VI and before the deposition of unit VII. All three fault zones in the trench cut to approximately the same level with similar degrees of soil development in the apparently unfaulted unit VII. It is possible that F1 and F2 ruptured together and F3 failed in a separate event. However, given the moderate quality of the stratigraphic and pedogenic ties across the trench, we favored the more conservative single-event interpretation. Rotated blocks of carbonate-cemented gravels from unit VI are present within the alluvial wedge sourced from unit V. The presence of unit VI gravels within the alluvial wedge indicates that the earthquake occurred well after the deposition and cementation of the base of unit VI. The OSL ages obtained from unit V provide a maximum age for faulting with a mean age of 20.6 ± 0.7 ka and the youngest single age of 18.4 ± 1.5 ka. A minimum age could not be directly determined because the only unit unaffected by faulting, unit VII, did not contain

material suitable for OSL analysis. It is reasonable, however, to correlate unfaulted unit VII to fluvial unit Qya2 elsewhere in the hanging wall of the Carrizal fault. Unit Qya2 has a mean age of 1.37 ± 0.87 and an oldest age of 6.02 ± 0.56 ka. Therefore, based on combined ages of units, and our assumption that the consistent level of rupture for all three fault traces in Trench 28 represents the Most Recent Earthquake (MRE), we conclude that it had a total vertical offset of 2.2 m and occurred between 20.6 ± 0.7 ka and 1.4 ± 0.9 ka, while using the individual ages the MRE occurred between 18.35 ± 1.53 ka and 6.02 ± 0.56 ka. Also note that the MRE occurred after unit VI, not the dated unit V, and therefore it occurred within an undefined younger part of age ranges given here.

The geologic relationships in the Bonfil quarry site can be interpreted as the result of 1–3 earthquakes (Fig. 8) sometime after the deposition of unit Hc. Unit Hc shows thickening toward the footwall, which indicates a depositional wedge likely formed in response to an earthquake (earthquake I). One interpretation is that the main wedge of unit Hc formed due to earthquake I did not include the irregular and lenticular upper part of Hc from distance 9.2–11.7 m and beyond (labeled as upper Hc on Fig. 6B). In this interpretation, deposition of the upper part of unit Hc continued after earthquake I, followed by stability and soil formation (Fig. 6B). The abundance of rootcasts in unit Hc may be indicative of a paleosol; however, many of the rootcasts do not appear to have formed in situ, which suggests they may have been eroded from the Comondú sandstone in the footwall and redeposited on the hanging wall following earthquake I. The lack of a well-preserved soil at the top of Hc indicates that the upper portion of this unit may have eroded. Unit Hb was deposited soon after this erosional event between 17.14 ± 0.96 and 18.14 ± 1.04 ka, or with a weighted mean age of 17.6 ± 0.71 ka (Fig. 8).

Earthquake II occurred after unit Hb was deposited, fractured unit Hb, and created space for the Ha colluvial wedge (Fig. 8). The small difference in soil development between the uppermost part of Hb and lower Ha indicates deposition of the wedge took place soon after stripping of the uppermost Hb. Earthquake II may have caused ~1 m of offset at this site in order to produce the accommodation space for the wedge. Earthquake III is the final and most recent earthquake we have interpreted, which was followed by deposition of the upper part of unit Ha. From detailed mapping near the Bonfil quarry, unit Ha is correlated with unit Qya3 with an OSL age of 8.58 ± 0.44 ka.

A more conservative reconstruction would be to combine event II and event III. That is, rather than earthquake II occurring before the deposition of the Ha colluvial wedge, there may have only been one earthquake that fractured unit Hb and triggered the deposition of the entire Ha colluvial wedge. In this conservative interpretation, the most recent earthquake occurred between 17.6 ± 0.71 ka and 8.58 ± 0.44 ka with an offset of ~1 m. The previous possible earthquake occurred soon before unit Hb with 17.14 ± 0.96 and 18.14 ± 1.04 ka ages and a mean of 17.6 ± 0.71 ka.

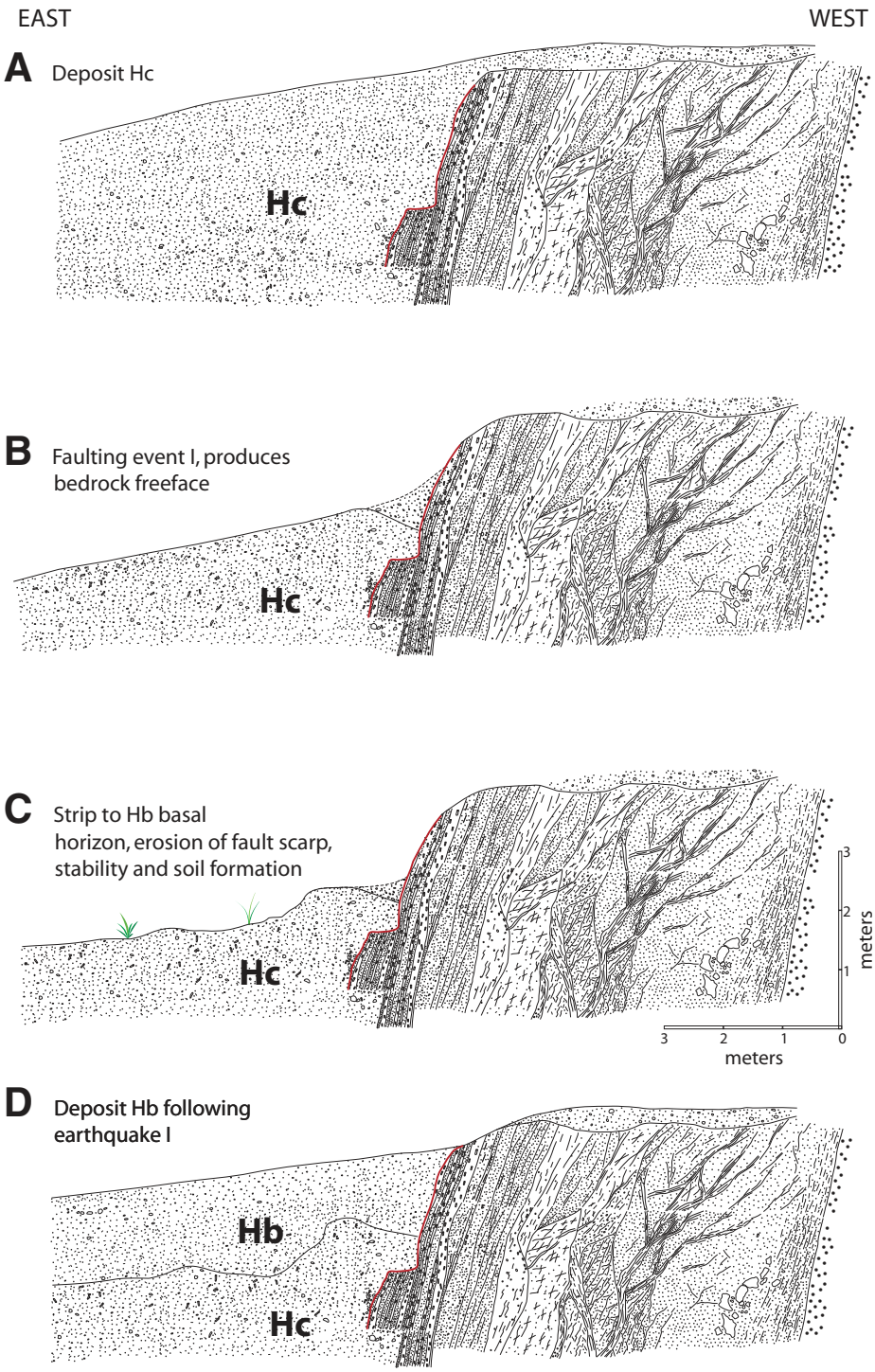

Figure 8 (*Continued on following page*). Sequence of events from an interpretation of the Bonfil quarry paleoseismic log. See text for discussion. We assume in this interpretation that faults F2 and F3 are relatively minor and slip with F1. See text for more explanation.

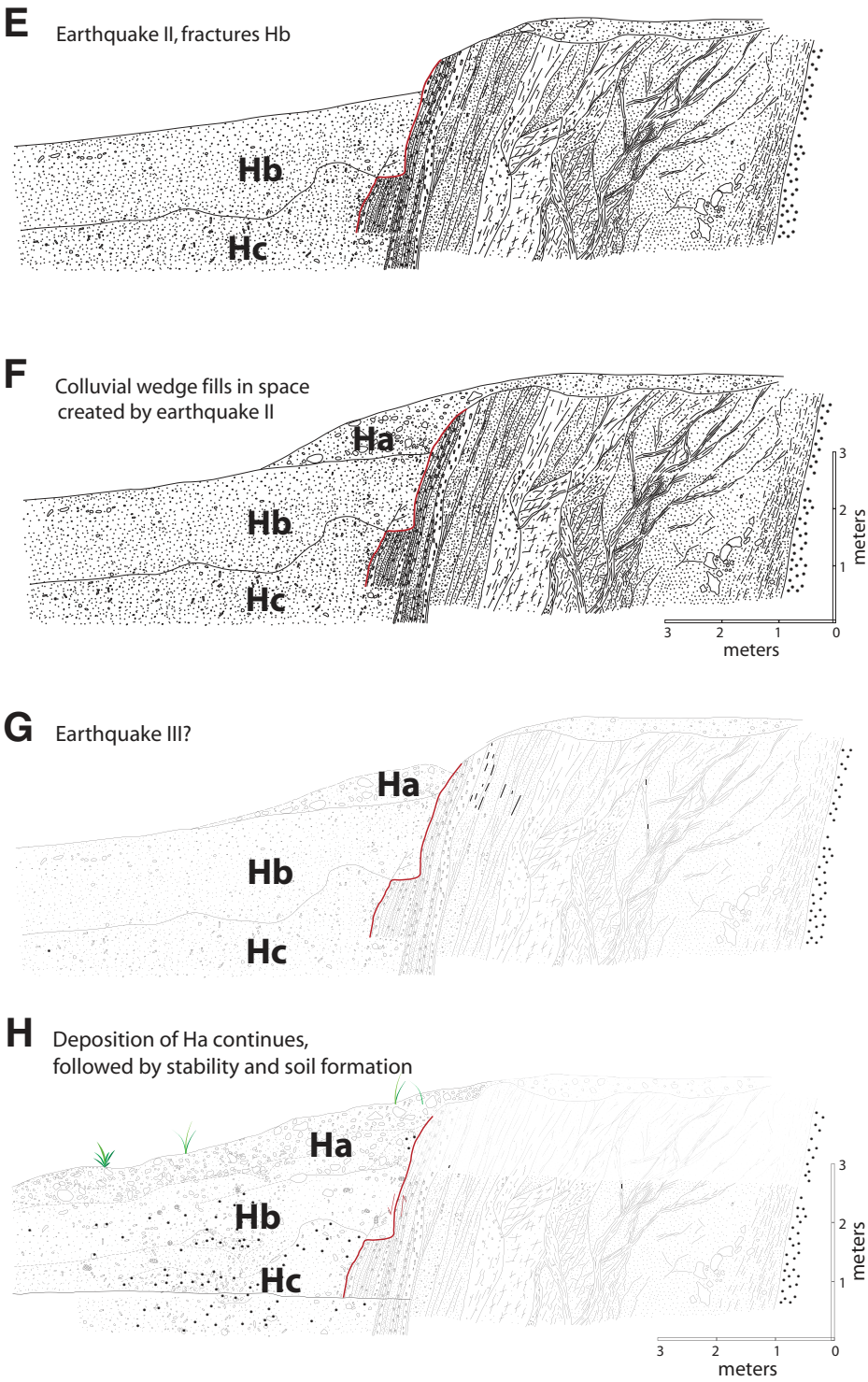

Figure 8 (*Continued*).

Slip-Rate and Earthquake Magnitude Estimates from Onshore Evidence

Because only one earthquake could be dated at each trench site, a recurrence interval could not be calculated. For that reason, slip rates calculated between the most recent earthquake and the present are maximum rates of 0.1–0.2–0.4 mm/yr. The more conservative end of the range of possible rates would be based on the assumption that the last earthquake occurred soon after the youngest dateable faulted unit (i.e., units V and Hb) was deposited, whereas the other end of the range of rates is based on the assumption that the last earthquake occurred just before the overlying unfaulted unit (i.e., units VII and Ha) was deposited. If unit Ha in the Bonfil quarry trench were deposited immediately after the most recent earthquake, then the oldest age of 10.39 ± 0.71 ka for unit Ha (equivalent to map unit Qya_3) would imply a higher slip rate of ~0.1–0.2 mm/yr. If the most recent earthquake occurred soon after unit Hb in the Bonfil quarry trench was deposited, then the youngest age of 17.14 ± 0.96 ka for this unit would imply a lower slip rate of 0.1 mm/yr. Therefore, the range of maximum slip rates at the Bonfil quarry site is 0.1–0.2 mm/yr. Likewise, at Trench 28, a slip rate of 0.4 mm/yr can be calculated from the older age of 6.02 ± 0.56 ka for unit VII (equivalent to map unit Qya_2), while a rate of 0.1 mm/yr is based on an earthquake soon after faulted unit V was deposited. Therefore, the range of maximum slip rates at Trench 28 is 0.1–0.4 mm/yr. Based on the bracketing ages provided by faulted and unfaulted sediment at both trench sites, the maximum slip rate along the onshore Carrizal fault may potentially range between 0.1 and 0.4 mm/yr, and ground rupturing earthquakes forming 1–2 m scarps would occur every ~2.5–20 ky.

We estimate the magnitude of paleoearthquakes on the Carrizal fault in two ways that result in a range of M 6.3 to 6.9. One model is a correlation between the most recent earthquake at Trench 28 with the most recent earthquake at the Bonfil quarry, which would imply that the most recent earthquake ruptured at least a 10 km length of the fault, the distance between the Bonfil quarry and Trench 28. A minimum normal fault surface rupture length of 10 km corresponds with a magnitude M ~6.3 earthquake and an average displacement that is less than 1 m (Wells and Coppersmith, 1994). However, the vertical displacement of unit VI at Trench 28 is ~2 m. An average displacement of 2 m coincides with a surface rupture length of ~40 km, which implies a magnitude M ~6.8 earthquake (Wells and Coppersmith, 1994). Alternatively, if we only use the fault offsets at our two sites, the colluvial wedges at the Bonfil quarry indicate possible surface ruptures of 1–2 m, while unit VI at the Trench 28 site is displaced ~2 m. If these displacement estimates are accurate, then earthquakes of M 6.7–6.9 are suggested along the northern Carrizal fault.

Uplifted Marine Terraces in Footwall of the Offshore Carrizal Fault

A coastal strip was mapped on the west side of La Paz Bay to study the uplifted marine terraces (Buchanan, 2010). At least four levels of

subhorizontal Quaternary uplifted marine terraces (QI, QII, QIII, and QIV) are present in the footwall of the offshore Carrizal fault along the coast for ~50 km (Fig. 9). The terraces are isolated, elongate surfaces ~50–300 m in length and stand 15–65 m above sea level. The highest QIV terraces are completely stripped of marine deposits and form small, rounded remnants that support little vegetation and commonly are partially covered by colluvial deposits. QIII terraces are commonly stripped of any deposits, but locally they contain marine deposits that vary from 0.2 to 0.8 m thick. The QIII deposits are poorly sorted, well rounded, and consist of boulders, pebbles, and cobbles with a matrix of shell hash, and gray, buff-colored coarse- to medium-grained sand.

Common QII, and less common, QI marine terraces are locally completely stripped of deposits but more commonly retain marine deposits. QII and QI marine deposits are poorly sorted, well-rounded pebbles to cobbles to boulders with a matrix of shell hash, and gray, buff-colored coarse- to medium-grained sand, and mollusk (most commonly *Chione*) shells. Marine fossils include bivalves, oysters, echinoid spines, algal debris, and sand dollar species. A few QII and QI terrace deposits include coral species, and a few QI deposits contain gastropods. The coral beds are typically 1.0–4.0 m thick and overlie mollusk-bearing beds. A seaward-thinning wedge of degraded bedrock colluvium, ranging from 0.5 to 20 m thick but commonly 5–6 m thick, is deposited on top of, and truncated against, most QII terrace deposits. Marine inner edges are locally well preserved. No QI terraces were found north of San Juan de la Costa.

Elevation and Age of Uplifted Marine Terraces and Coastal Uplift Rates

Over 150 local exposures of the four marine terrace levels were measured for elevation, and ten marine terrace deposits with shells were analyzed using the amino acid racemization (AAR) method (Fig. 9) (Buchanan, 2010). The elevation of terraces was measured along transects using a Brunton compass, a hand-held Berger level, and measuring tape (nine transects that include 18 terraces), or at a single site using a hand-held GPS barometrically calibrated to mean sea level (135 sites; the 18 other terraces were also measured with GPS); the results of the two methods were comparable within <5%. These methods are not accurate enough to detect subtle trends in elevation change of the marine terraces along the coastal belt.

The average elevations of the four subhorizontal Quaternary uplifted marine terraces are: (1) 57 ± 7 m (22 QIV terraces; all in the southern area); (2) 41 ± 4 m (33 QIII terraces; 32 in south, 1 in north); (3) 22.6 ± 2.3 m (78 QII terraces; 58 in south, 20 in north); and (4) 16.6 m (20 QI terraces, all in the south). Below we refer to a terrace Q0, which is not part of the flight of uplift marine terraces on the west side of La Paz Bay discussed here. Instead terrace Q0 is the lowest footwall surface west of the onshore Carrizal fault shown in profile 1 in Figure 4C. The southern area is a relatively steep coastline that included 132 terrace exposures, all within 1–2 km of the coast. The northern area is a much less steep coastal belt that included 21 terraces in this study; all lie within 2 km of the coast (Fig. 9).

The age of formation of the uplifted marine terraces is estimated by correlating AAR ratios of mollusk shells with independently derived U-Th ages from the same latitude (e.g., Kennedy et al., 1982; Muhs et al., 1990; Wehmiller and Miller, 2000). The U-Th age control for QII terraces in the study area is from *Porites panamensis* corals from three terraces in the northern area that were dated by DeDiego-Forbis et al. (2004). In the present study, *Chione* mollusk shells were collected from these same three terraces, within ~2 m of the collection sites of the coral. DeDiego-Forbis et al. (2004) reported U-Th ages of 109–209 ka on the corals, which had initial ^{234}U values in excess of modern seawater, indicating an open system and uncertainty in the ages. Therefore, DeDiego-Forbis et al. (2004) used the approach of Gallup et al. (1994), which resulted in terrace ages of 128 ± 2 ka. Sirkin et al. (1990) used U-Th techniques to date *Porites* coral from an 8-m-high marine terrace deposit in Arroyo del Coyote on the east side of La Paz Bay (COY009 on Fig. 9) that was also analyzed for AAR in this study and is part of the set of QII terraces. Sirkin et al. (1990) calculated an age of 123 ± 6 ka for the coral, within analytical uncertainty of the DeDiego-Forbis et al. (2004) age.

Because three mollusk samples from this study were collected from the same U-Th dated terraces of DeDiego-Forbis et al. (2004), we assume that these QII terraces from our study are directly dated at 128 ± 2 ka, indicating that they formed during MIS 5e. The average Asp THAA D/L ratios for the shells from the three terraces are 0.765 ± 0.040, 0.769 ± 0.010, and 0.783 ± 0.026, respectively, and they have a combined age 0.772 ± 0.009 (Table 4). This value is used as the control datum for which the other AAR ages are compared. A fourth sample location from another QII terrace in the northern area is interpreted as a MIS 5e terrace because of its elevation, and it has a similar average Asp THAA D/L ratio of 0.775 ± 0.027 (sample QMt 77, Table 4).

The ages of QII marine terraces in the southern area are correlated by AAR analysis with QII terraces in the northern area. Average Asp THAA D/L ratios on shells from five QII terraces (Qmt in Table 4) in the southern area are 0.774 ± 0.029, 0.787 ± 0.014, 0.772 ± 0.019, 0.772 ± 0.020, and 0.785 ± 0.024 (Table 4) with an average Asp D/L ratio of 0.778 ± 0.007. This result is consistent with the average Asp D/L ratios of the three samples from near the U-Th age of 128 ka in the northern area, 0.772 ± 0.009, suggesting that these terraces are also MIS 5e. The average Asp THAA D/L ratio of all shell samples that we analyzed from the QII terraces in the coastal belt on the west side of La Paz Bay is 0.776 ± 0.008.

The average Asp THAA D/L of our sample from the 8-m-high terrace of Sirkin et al. (1990) is 0.763 ± 0.015 (sample COY009 in Table 4), equivalent within error to the average Asp D/L ratio of the U-Th dated terraces of DeDiego-Forbis et al. (2004). Furthermore, the average Asp D/L ratio of the 9-m-high terrace of Halfar (1999) is 0.778 ± 0.029 (sample BONZ in Table 4), also similar to the AAR results from the U-Th dated terraces in the northern area. Halfar (1999) dated this terrace to be 142 ± 2 ka but suggested it may be a MIS 5e terrace.

The southernmost terrace in our southern area containing *Chione* shells is from terrace QI-B, and gave an average Asp THAA D/L ratio of 0.711 ± 0.070 (Table 5). This ratio is lower than the results from samples from the QII terraces in our study, although it overlaps a small amount within error. Sample QI-B comprises four *Chione* shells. Pitting and scrapping were noted on shell 4 of this sample, and analyses suggest that shell 4 is a relatively older shell re-deposited into the lower QI-B deposit (Table 5). Reworked mollusk shells have been documented by Halfar (1999) on Isla Espiritu Santo, 40 km east of the Carrizal fault in the La Paz Bay, and DeDiego-Forbis (2004) in our northern area. The average Asp D/L ratio of 0.790 ± 0.01 for shell 4 (Q1-B-4 on Table 5) agrees with the samples from the U-Th dated QII terraces and verifies reworking of the shell from an older deposit into deposit QI-B as an explanation for the pitted shell. When sample QI-B is analyzed with only the three remaining shells, the resulting average Asp D/L ratio of 0.691 ± 0.037 (Table 5) is significantly lower than the average AAR results from the QII terraces (0.776 ± 0.008, Table 4). Therefore, the QI-B terrace is younger than MIS 5e and probably correlated with MIS 5c or MIS 5a. The concentration ratios of amino acids Ala/Asp increase with age because Ala is a more stable amino acid than Asp and is formed through the decomposition of Thr (Bada, 1991). The average Ala/Asp concentration for terrace QI-B

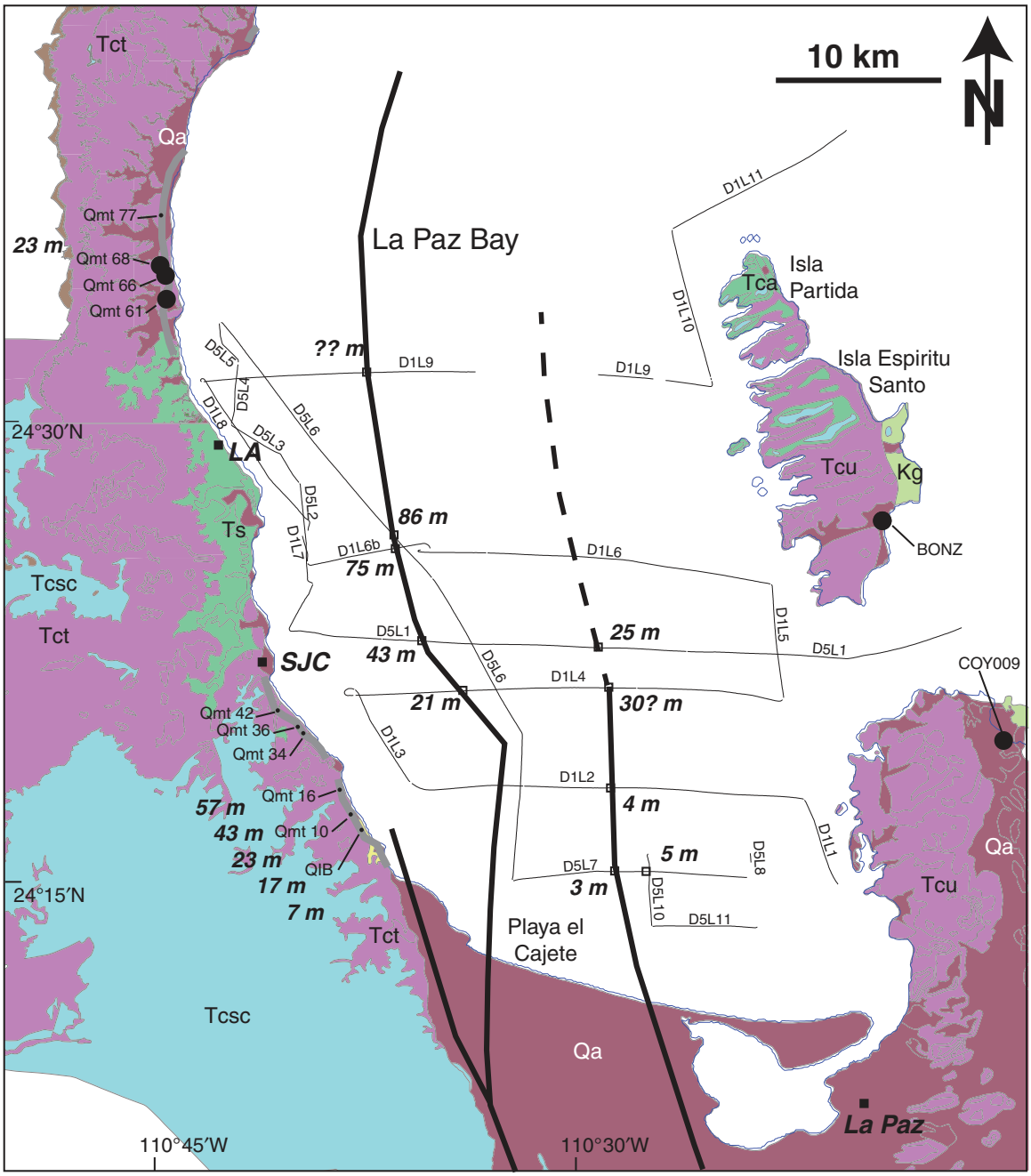

Figure 9. Geologic map of the onshore area around La Paz Bay, the Quaternary uplifted marine terraces from this study (Qmt), and the compressed high-intensity radar pulse (CHIRP) lines with the offshore fault scarp locations (small squares). The gray lines along the coast are the northern and southern study areas that included all the terraces. Fault scarp heights are shown near scarp locations. The elevations of the uplifted marine terraces from this study are shown: one terrace in the north and five terrace elevations in the south. Terraces BONZ and COY009 on the east side of La Paz Bay are from other studies (Halfar, 1999; DeDiego-Forbis et al., 2004). Uplifted marine terraces with U-Th ages are shown as filled black circles. Map unit abbreviations: Kg—Cretaceous granite; Qa—Quaternary alluvium; Qmt—Quaternary marine terrace; Tca—Tertiary Comondú Group andesite; Tcsc—Tertiary Comondú Group sandstone and conglomerate; Tct—Tertiary Comondú Group tuff; Tcu—Comondú Group undifferentiated; Ts—Tertiary sedimentary marine units older than the Comondú Group.

TABLE 4. SUMMARY OF *CHIONE* AMINO ACID RACEMIZATION DATA

Lab ID (UAL-)	Sample	Depth (m)	U-Th (ka)	n*	D/L Asp	1σ	D/L Glu	1σ	n*	A/I	1σ
Conventional THAA											
6017	QI-B	1.0–1.4		3	0.691	0.037	0.713	0.038			
6017	QI-B	1.0–1.4		1†	0.790	0.011	0.798	0.010			
6018	Qmt 10	1.4–1.5		2	0.774	0.029	0.706	0.004			
6019	Qmt 16	1.2–1.4		4	0.787	0.014	0.734	0.013			
6023	Qmt 34	1.8–2.0		5	0.772	0.019	0.703	0.026			
6022	Qmt 36	1.0–1.2		3	0.772	0.020	0.705	0.055			
5812	Qmt 42	1.3–1.5		5	0.785	0.024	0.766	0.030	5	0.734	0.068
5809	Qmt 61	1.7–2.0	128	5	0.765	0.040	0.738	0.086	5	0.847	0.005
5810	Qmt 66	1.3–1.5	128	5	0.769	0.010	0.757	0.020	5	0.683	0.061
5815	Qmt 68	1.2–1.5	128	5	0.783	0.026	0.748	0.035	5	0.731	0.123
5814	Qmt 77	1.0–1.2		4	0.775	0.027	0.781	0.043	5	0.964	0.039
5811	COY009	1.4–1.6		5	0.763	0.015	0.772	0.025	5	0.915	0.069
5813	BONZ	0.5–0.6		5	0.778	0.029	0.751	0.061	5	0.792	0.155
Intra-Crystalline THAA											
6247		1.7–2.0	128	5	0.770	0.030	0.700	0.030			
6246		1.3–1.5	128	5	0.798	0.016	0.750	0.036			
6245		1.2–1.5	128	5	0.801	0.021	0.723	0.038			
Intra-Crystalline FAA											
6247		1.7–2.0	128	5	0.856	0.050	0.831	0.042			
6246		1.3–1.5	128	5	0.876	0.012	0.857	0.012			
6245		1.2–1.5	128	5	0.895	0.024	0.830	0.019			

Note: D/L—ratio of D- to L-amino aciden enantiomers; Asp—aspartic acid; Glu—glutamic acid; THAA—total hydrolysable amino acids; FAA—free amino acids.
*Number of subsamples used to calculate mean ratio.
†Reworked sample.

shells is 0.500 and for shells from QII terraces is 0.958, further indicating that the QI-B terrace is a younger terrace. Finally, the elevation of QI-B is ~6 m lower than the average elevation of the QII terraces in our study.

We assume that the three QII terraces in the northern area have a U-Th age of 128 ka (DeDiego-Forbis et al., 2004), and this age was used with the average Asp THAA D/L ratio of 0.772 (from this study) from the same terraces in the parabolic equation as the control datum for which the ages from the terraces in the southern area were derived. The resulting ages from the parabolic equation (where mc = 2.16×10^{-3}) for the samples from the southern area of this study are shown in Figure 10. On the basis of the calibrated rate of AAR, the range of ages for QII terraces from this study is 128 to 133 ka. The AAR-derived ages of the QII terraces agree with the U-Th dated terraces of Sirkin et al. (1990) and Halfar (1999), and other terraces in the Baja California region (Ortlieb, 1991; Mayer and Vincent, 1999; Macy, 2005). In contrast, the average AAR age for the lower QI-B terrace from the parabolic analysis is 103 ka (Fig. 10). This suggests that terrace QI-B was formed during MIS 5c.

When the elevations and ages of marine terraces QI and QII are combined with estimates of sea level at each MIS, uplift rates along the west side of La Paz Bay can be calculated. Interglacial highstands have occurred globally at ~80, 105, 125, 200, 320, and 420 ka, corresponding to MIS 5a, 5c, 5e, 7, 9, and 11, respectively, and Table 6 shows the highstand elevations we used under the terrace ages.

The predicted rate of uplift of the western coast of La Paz Bay can be calculated (Table 6). From this analysis, we suggest that the undated terraces Q0, QIII, and QIV were formed during MIS 5a, 9, and 11, respectively. If the QI and QII terraces are assumed to be MIS 5c and 5e from our study, then the rates of uplift of the five marine terraces vary from ~0.1 to 0.2 m/ky. The most robust result is that terrace QII has an uplift rate of 0.13 m/ky since 128 ka (Table 6). Given the uncertainties in the elevation of the higher QIII and QIV terraces with fewer well-defined inner edges (and therefore these rates may be underestimates) and the uncertainty in the elevation of older highstands, our data suggest a constant uplift rate of 0.1–0.2 mm/yr for the footwall of the Carrizal fault since ca. 500 ka.

TABLE 5. SUMMARY OF *CHIONE* AMINO ACID RACEMIZATION DATA FOR QI-B TERRACE

Lab ID (UAL-)	Sample		D/L Asp	D/L Glu	D/L Ser	D/L Ala
Initial analysis						
6017 A	QI-B-1		0.734	0.760	0.338	1.097
6017 B	QI-B-2		0.668	0.664	0.115	1.090
6017 C	QI-B-3		0.643	0.706	0.153	1.084
6017 D	QI-B-4		0.798	0.791	0.121	1.109
		Average	0.711	0.730	0.182	1.095
		Std dev	0.070	0.056	0.105	0.011
		Cv	9.8	7.7	58.0	1.0
Re-analysis						
6017E	QI-B-1		0.735	0.712	0.397	1.087
6017 F	QI-B-2		0.688	0.754	0.474	1.103
6017 G	QI-B-3		0.679	0.683	0.380	1.065
6017 H	QI-B-4		0.782	0.805	0.285	1.083
		Average	0.721	0.739	0.384	1.085
		Std dev	0.048	0.053	0.078	0.016
		Cv	6.7	7.2	20.3	1.5
Reworked or re-deposited shells, correlated with QII terraces						
6017 D	QI-B-4		0.798	0.791	0.121	1.109
6017 H	QI-B-4[a]		0.782	0.805	0.285	1.083
		Average	0.790	0.798	0.203	1.096
		Std dev	0.011	0.010	0.116	0.018
		Cv	1.4	1.3	57.1	1.6
Correlated with QI terraces						
6017 A	QI-B-1		0.734	0.760	0.338	1.097
6017 E	QI-B-1[a]		0.735	0.712	0.397	1.087
6017 B	QI-B-2		0.668	0.664	0.115	1.090
6017 F	QI-B-2[a]		0.688	0.754	0.474	1.103
6017 C	QI-B-3		0.643	0.706	0.153	1.084
6017 G	QI-B-3[a]		0.679	0.683	0.380	1.065
		Average	0.691	0.713	0.310	1.088
		Std dev	0.037	0.038	0.143	0.013
		Cv	5.3	5.3	46.1	1.2

Note: D/L—ratio of D- to L-amino acid enantiomers; Asp—aspartic acid; Glu—glutamic acid; Ala—alanine; Cv—coefficient of variation (std dev / average) x 100; Std dev—standard deviation.
*Re-analyzed subsamples used in final D/L ratio average.

UAL	Terrace	Avg Asp $(D/L)_s$	AAR Age (ka)
6018 A, B, C, D, E, F, G	QI-B	0.691	103
6017 D, H	QI-B	0.790	110
6018 A, B	Qmt 10	0.774	128
6019 A, B, C, D	Qmt 16	0.787	133
6023 A, B, C, D, E	Qmt 34	0.772	128
6022 A, B, C	Qmt 36	0.772	128
5812 A, B, C, D, E	Qmt 42	0.785	132
5814 A, B, D, E	Qmt 77	0.775	129

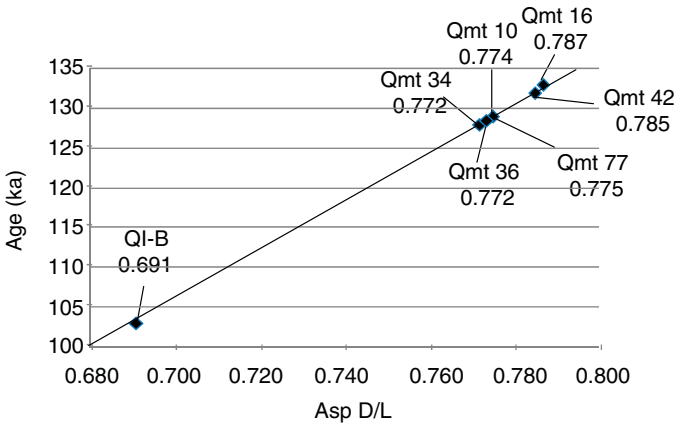

Figure 10. (A) Table of age estimates for *Chione* from QI and QII terraces using apparent parabolic kinetics. DeDiego-Forbis et al. (2004) dated terraces Qmt 61, 66, and 68 (near terrace Qmt 77 of this table) using U-Th analysis, and reported an average age of 128 ka. Qmt 61, 66, and 68 were dated independently in this study using amino acid racemization (AAR) analysis of *Chione*. Qmt 61, 66, and 68 terrace ratios averaged 0.772 ± 0.03 and were used as the control datum for which the other terrace's ages were derived. (B) Range of predicted ages of the QI and QII terraces using the parabolic equation. The *x*-axis is the Asp D/L in the sample of unknown age. The *y*-axis is the predicted age, where mc = 2.16 × 10^3.

TABLE 6. UPLIFT RATES AND ELEVATIONS OF MARINE TERRACES

Assumed uplift rates (m/ka)	Predicted terrace elevations (m)					
	80 ka −5 m	105 ka −2 m	128 ka +6 m	200 ka −10 m	320 ka +4 m	420 ka +20 m
0.08	1.4	6.4	16.2	6.0	29.6	53.6
0.09	2.2	7.5	17.5	8.0	32.8	57.8
0.10	3.0	8.5	18.8	10.0	36.0	62.0
0.11	3.8	9.6	20.1	12.0	39.2	66.2
0.12	4.6	10.6	21.4	14.0	42.4	70.4
0.13	5.4	11.7	22.6	16.0	45.6	74.6
0.14	6.2	12.7	23.9	18.0	48.8	78.8
0.15	7.0	13.8	25.2	20.0	52.0	83.0
0.16	7.8	14.8	26.5	22.0	55.2	87.2
0.17	8.6	15.9	27.8	24.0	58.4	91.4
0.18	9.4	16.9	29.0	26.0	61.6	95.6
0.19	10.2	18.0	30.3	28.0	64.8	99.8
0.20	11.0	19.0	31.6	30.0	68.0	104.0
0.21	11.8	20.1	32.9	32.0	71.2	108.2
This study		16.6	22.6		41.0	57.1
Terraces south of study area	7.2	18.0	27.0			57.0
Quaternary terrace	Q0	QI	QII		QIII	QIV

Results—Marine Paleoseismic Survey

Offshore paleoseismic data were collected from La Paz Bay using submeter-resolution, seismic CHIRP in August 2008 (Fig. 11). Several of the CHIRP lines from La Paz Bay had poor or no data below the seafloor, but five profiles showed east-facing bathymetric steps interpreted as fault scarps of the northern Carrizal fault, and four bathymetric steps are interpreted as the northern Centenario fault (Fig. 11). Locally, CHIRP lines do show layering below the seafloor. The presumed fault offsets shown on the bathymetric steps ranges from ~21 to 86 m (and possibly more to north on line D1L9) on what is interpreted as the Carrizal fault and 3–5 m on the Centenario fault.

It is not certain that all of the bathymetric steps are fault scarps, but the preponderance of evidence leads us to conclude that they are. First, lines D5L6, D1L6b, and possibly D1L9 show a fault-related wedge of sediment thickening toward the base of the scarp; line D5L1 shows two faulted wedges east of the base of the scarp (Fig. 11). The wedges are 5–30 m thick at their thickest at the west edges, which in some cases may be a minimum because the CHIRP lines are not clear. Second, in map view, the scarps form a smooth, curved line that approximately mimics the coastline to the west, and they all lie 8–10 km from the west coast of the bay (Fig. 9). This alignment is what would be predicted for an offshore fault and makes a logical northward projection of the onshore Carrizal fault with a splay near the southwest coast of the bay (Fig. 2). Third, the scarps increase in height from south to north. This trend could indicate that the scarps are getting older to the north as discussed below, or it may indicate that there is a higher rate of faulting to the north. The latter interpretation is supported by the observation that the largest scarps are due east of the coastal belt with the oldest strata (Fig. 9). Note that the west coast of La Paz Bay forms a broad arch in the strata. There is a belt of the oldest Tertiary marine strata (Ts on Fig. 9) from approximately San Juan de la Costa north to Las Animas with progressively younger Tertiary strata of the Comondú Group north and south of this belt. This pattern in the footwall of the Carrizal fault suggests that the area with the oldest strata has the largest total offset on the Carrizal fault. Lastly, the 21 m scarp of the Carrizal fault on the southernmost CHIRP line D1L4 compares favorably with the 11–17 m height of the four fault scarps along the onshore Carrizal fault within 10 km of the bay (profiles 1–4 on Fig. 4C, and Maloney, 2009), which supports our interpretation that the onshore Carrizal fault links to the north to the fault defined by the 5–6

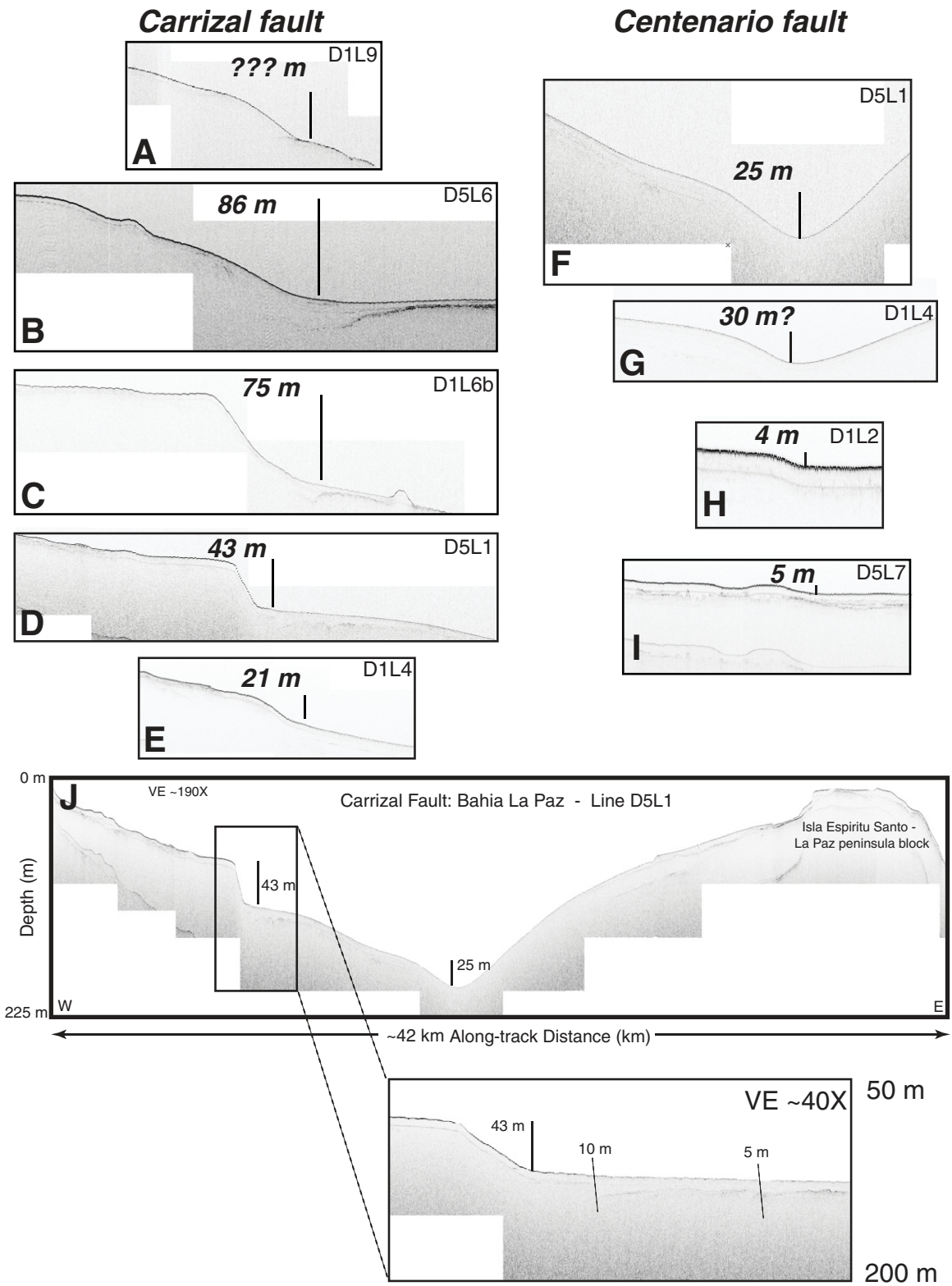

Figure 11. (A to I) Compressed high-intensity radar pulse (CHIRP) profiles across possible fault scarps in La Paz Bay across the Carrizal and Centenario faults. Profile J is the total profile of line D5L1 with 190× vertical exaggeration suggesting that the low-angle, 43-m-high, east-facing step is a fault scarp. Note the enlarged area below that shows clear offset of the sedimentary horizons in the CHIRP profile highlighting that there are 10 m and 5 m fault offsets in the hanging wall just east of the 43-m-high scarp. See text for more discussion of these inferred fault scarps. VE—vertical exaggeration.

fault scarps on the western side of La Paz Bay (Fig. 2).

The following observations may be more difficult to explain as fault scarps and are explored in the Discussion section. The scarps are subtle features with a slope of ~1°; however, this is considerably steeper than the 0.2° slope of the rest of the west side of the bay (Fig. 11). The offshore fault scarps are 8–10 km offshore from the uplifted marine terraces near the coastline to the west, 3–12 km south of San Juan de la Costa, and 24–30 km north of San Juan de la Costa.

The top of the 43- and 21-m-high scarps is at ~80 m deep below sea level. The higher 75–86 m fault scarps to the north are under >120 m of water and have no control on their age. Sea level reconstructions since the last glacial maximum suggest that rising sea level passed the 80 m depth of these scarps at ~14,000 years ago (Fleming et al., 1998). If we assume that rising sea level would have eroded and leveled a scarp on the seafloor, it is unlikely that these fault scarps formed before 14,000 yr B.P. These observations and assumptions suggest that there has been a late Quaternary slip rate on the offshore Carrizal fault of 1.5–3 mm/yr, which is significantly higher than the 0.13 mm/yr long-term rates suggested for the uplifted marine terraces to the west in the footwall of the Carrizal fault. However, given the low slope on these submerged scarps, it seems likely that they were partially leveled and record a pre-14,000 and post-14,000 history, and thus we conclude that they do not give us information on the age and rate of faulting. Coring and dating of the fault wedges would be required to obtain such information, and lacking that data, we discount the suggested 1.5–3 mm/yr faulting rates.

Four bathymetric steps are interpreted as fault scarps along the northern Centenario fault, but this is a more tenuous interpretation (Fig. 11). They all form east-facing steps in the seafloor of reasonable height to be scarps (Fig. 11). Line D5L7 also has a possible ~3-m-deep graben west of the main scarp (Fig. 11). However, the higher 25 and 30 m scarps on lines D1L4 and D5L1 to the north end into the deepest part of the bay on each line and are therefore more difficult to evaluate. And when line D5L1 is viewed as a whole (Fig. 11), the possible eastern scarp (Centenario fault?) has a much lower slope than the western scarp. Finally, none of these Centenario fault scarps have the fault wedges that are in the hanging wall of the Carrizal fault scarps. In support of the Centenario fault scarps, they form a south to north alignment and are also along the offshore projection of the onshore Centenario fault (Fig. 2). The small scarp heights in the south also fit with the subtle to no scarps along the Centenario fault onshore. Finally, microseismicity is common near and just east of the Centenario fault near the coastline and scattered offshore (Fig. 3).

DISCUSSION

Summary of Faulting Rates

This study combines three types of data that bear on the rate of faulting in the late Quaternary (since ~500 ka) on the Carrizal fault. Uplifted marine terraces along the western side of La Paz Bay are the most robust data for rates and give a coastal uplift rate of 0.13 mm/yr since MIS 5e at 128 ka and 0.1–0.2 mm/yr since MIS 11 at 420 ka. If we assume that uplift rates of terraces would approximate horizontal rates of faulting along moderately dipping faults, then the 0.1–0.2 mm/yr is relevant for extensional faulting rates as well (we have no information on the dip of the faults). The trenches along the onshore Carrizal fault include one earthquake in Trench 28 with 2.2 m offset, and 2–4 earthquakes in the Bonfil quarry road exposure with ~0.5–1 m offset on each earthquake. Data from both trenches suggest dip-slip offset rates of 0.1–0.2–0.4 mm/yr. Based on these data, the Carrizal fault may have a nearly constant rate of offset since 420 ka of 0.13 mm/yr, or more conservatively, 0.1–0.2 mm/yr all along the 80 km of the fault we studied. There are no data to indicate faulting rates on the Centenario fault, but the lesser scarp heights and lack of significant scarps in the onshore suggest it has faulting rates <0.1 mm/yr.

There is a provocative observation on the heights of the offshore scarps that may add further support for a constant faulting rate, if we assume that they survived erosion during the rising sea level after the last glacial maximum, which may explain their low scarp angle. The offshore scarps with heights of 21 and 43 m are identical within error to the elevation of the MIS 5e and MIS 9 marine terraces that also lie immediately to the west (Figs. 9 and 11). If we conclude based on these observations that the offshore scarps were preserved since the peak of increasingly older sea-level highstands moving northward, then the 21, 43, 75, and 86 m scarps formed at the MIS 5e, 9, 11, and 11 highstands, respectively. This possible tie from the offshore scarps to specific uplifted marine terraces along the coast suggests that (1) the constant faulting rate of 0.12–0.15 mm/yr is robust, and (2) there is no significant faulting between the offshore scarps and the coast. The latter conclusion is supported by the CHIRP lines as many of them ended within 1–2 km of the coast at only 10–20 m water depth, so we are suggesting that no significant scarps can lie between the end of those lines and the beach.

Fault Evolution in the La Paz Region

We can update the model of fault evolution in the La Paz region (Busch et al., 2011) based on our new data and the gravity line presented by Busch et al. (2011). One hypothesis concerning the long-term pattern of faulting of the Carrizal fault is that the fault is at a maximum total displacement offshore near and north of San Juan de la Costa because that is where the oldest rocks are exposed (Eocene–Oligocene marine strata), and those rocks lie near the middle of the broad arch formed by layered rocks in the footwall of the fault (Drake, 2005; Buchanan, 2010). In addition, in a simple interpretation one can project the 12° west tilts on the Comondú Group rocks on Espiritu Santo Island under La Paz Bay to the Carrizal fault, and that suggests a 2- to 3-km-thick basin (Fig. 12 and Puchalski, 2002). The addition of the northern Centenario fault within that basin from this study complicates that simple view of the bay. These observations are consistent with the offshore Carrizal fault being a large, tens-of-kilometers–long fault that grew laterally (e.g., Cowie and Scholz, 1992; Dawers and Anders, 1995).

If the Carrizal fault is in fact at a displacement maximum within the ~20 km north of San Juan de la Costa, then either the fault slips at a higher rate in that area, or the offshore component of the Carrizal fault in La Paz Bay is older than the fault to the south onshore. For the late Quaternary, we can eliminate the first hypothesis because faulting rates from our data are approximately the same from the south to north.

The hypothesis that the Carrizal fault is older in the north is supported by a gravity survey across the onshore faults west of La Paz (Busch et al., 2011). The hanging wall of the onshore Carrizal fault is the La Paz basin with a maximum gravity anomaly of ~10 mGal. The La Paz basin has a maximum depth to bedrock of ~500 m in the preferred four-layer gravity model. The gravity model shows a broad shallow basin with two subbasins separated by a bedrock high. The exposed geology of the La Paz basin south of the gravity line supports this because the Garambullo hills are a high of older Quaternary deposits with two distinct basins on either side (Fig. 4A). The westernmost of the two smaller basins on the gravity line is controlled by the east-dipping Carrizal fault on its western side, whereas the easternmost basin is controlled by the east-dipping Centenario fault on its western side. The deeper of the two basins is the Centenario basin with approximate maximum depths of 490 m in the four-layer model, while the basin adjacent to the Carrizal fault is only 250–300 m deep. The conclusion that the basin along

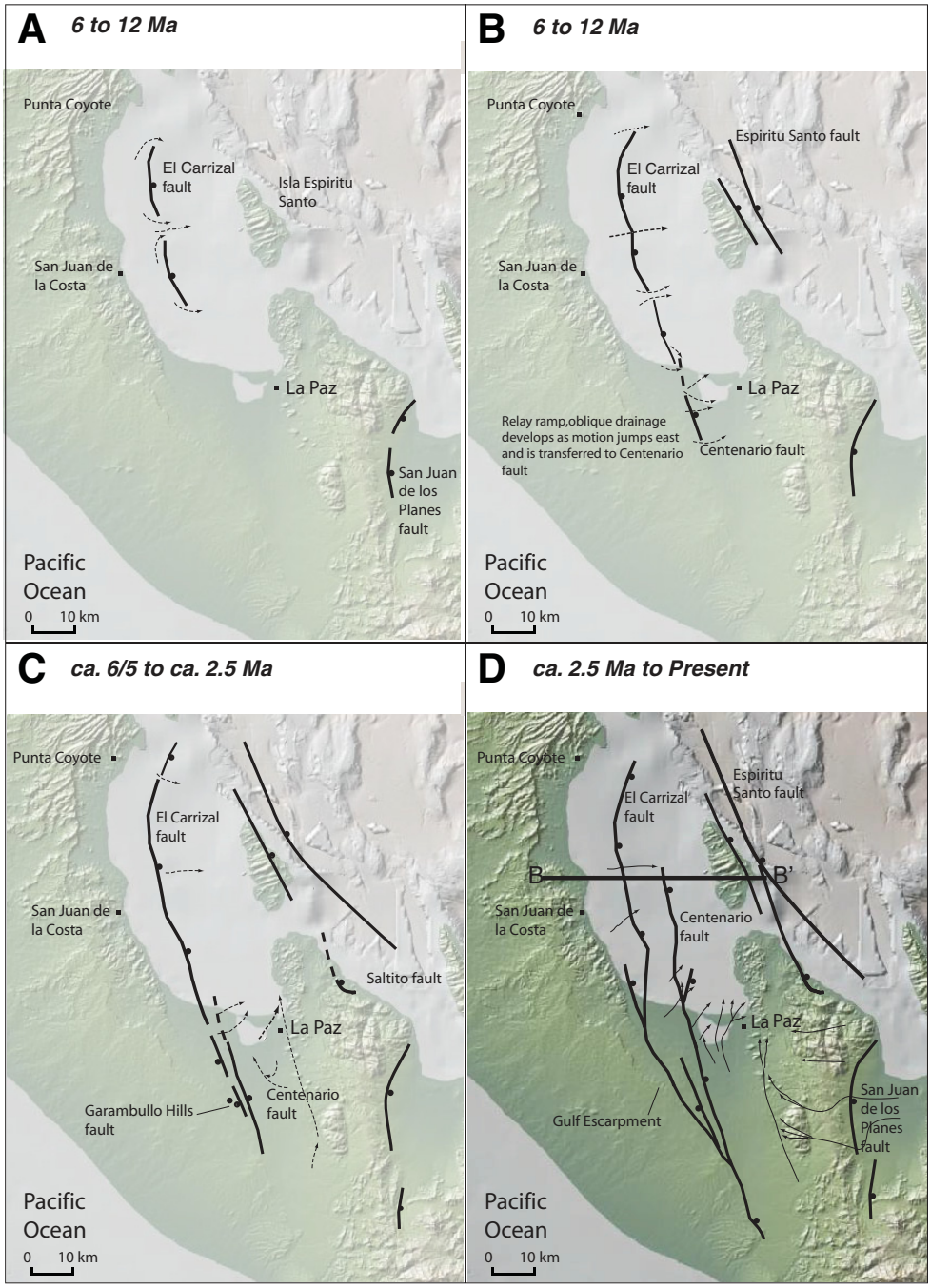

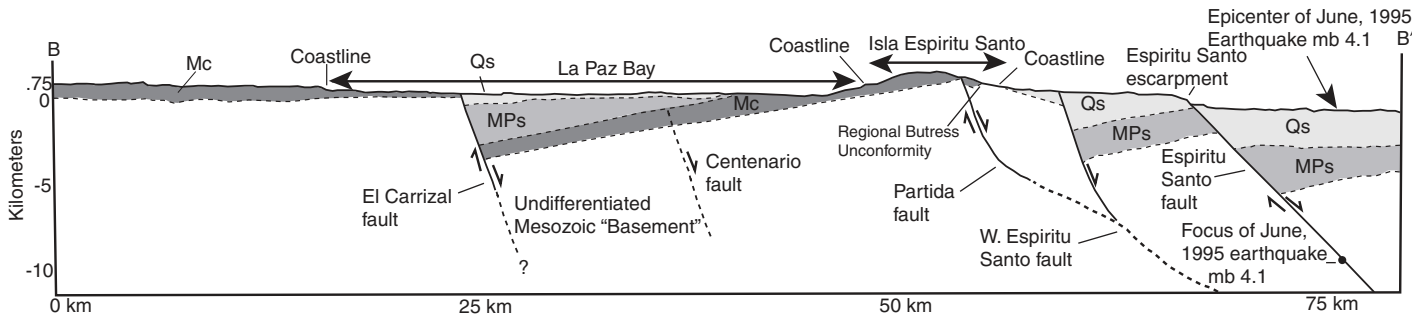

Figure 12. Proposed evolution of faulting in La Paz Bay region and an east-west cross section across the El Carrizal fault, the northern end of the Centenario fault, and across Espiritu Santo island to the Espiritu Santo fault system. See text for discussion.

the onshore Carrizal fault is shallower than the basin along the Centenario fault is not predicted by other geology. All surface geologic information and paleoseismology along the two faults from our study suggests that the Carrizal fault is the longer and more active of the two faults.

Our favored interpretation of the fault evolution in La Paz area (Fig. 12) (Maloney, 2009; Busch et al., 2011) is that the onshore Carrizal fault is younger than both the offshore Carrizal fault and the Centenario fault. The other key observation from our multiple studies is that there is a consistent late Quaternary rate of faulting on the onshore and offshore Carrizal fault that suggests strongly that it has been operating as one, ~100-km-long fault system for at least tens of thousands of years and likely for at least 100–200 ky. These inferences lead to the following scenario.

Subduction-related arc volcanism in southern Baja California ceased by 12 Ma (Hausback, 1984; Stock and Hodges, 1989; Umhoefer et al., 2001), and gulf-related extension along the former arc occurred starting in the ca. 12–6 Ma period (Lonsdale, 1989; Stock and Hodges, 1989; Fletcher et al., 2000). After 12.5 Ma, Pacific–North America plate motion became highly oblique to the former volcanic arc, causing plate boundary displacement to be oblique divergent (Stock and Hodges, 1989; Atwater and Stock, 1998). Therefore, based on the regional evidence, it is logical to assume that slip along the Carrizal fault began sometime between 12 and 6 Ma in the offshore segment of the fault (Fig. 12A). The presence of pre–Comondú Group marine strata in the footwall of the offshore Carrizal fault, the arched older strata, and the possible kilometer-scale offset on the offshore fault, all suggest that faulting initiated offshore near and north of San Juan de la Costa (Fig. 12A and cross section). Because the footwall rocks become younger south of San Juan de la Costa, and based on the gravity survey, it is likely that the Carrizal fault attained its final length during the later stages of development.

In a second stage of faulting, we speculate that motion on the Carrizal fault grew southward to the incipient Centenario fault (Fig. 12B). Offshore slip along the Carrizal fault continued. This faulting scenario is suggested by the gravity model (Busch et al., 2011) that shows that the onshore Centenario subbasin is thicker than the onshore Carrizal subbasin (Fig. 12). This gravity model leads us to interpret that the Centenario fault is older than the onshore Carrizal fault.

In a third stage, the Garamullo fault formed as an antithetic, west-dipping fault west of the Centenario fault in a step-over relation with the older offshore Carrizal fault (Fig. 12C). We also show the offshore Carrizal fault growing laterally to its present length.

Based on the estimated age of the onshore Carrizal subbasin interpreted from the gravity data (250- to 300-m-thick basin) and the rates of faulting from this study (0.1–0.2 m/ky maximum), we suggest that the onshore Carrizal fault formed at ca. 2–3 Ma. This is approximately the same time as faulting in the whole gulf-margin fault system slowed greatly, based on data from the San Jose Island basin at the northern end of La Paz Bay where faulting slowed at 2.5–2.4 Ma (Umhoefer et al., 2007) and based on the timing of the initiation of the full modern rates of spreading on the Alarcon rise at 2.4 Ma (Sutherland, 2006; Sutherland et al., 2012).

During this ca. 2.5–0 Ma stage (Fig. 12D), slip along the Garambullo Hills and Centenario faults ceased or slowed considerably, and the majority of east-west–directed strain in the onshore area was transferred to the onshore Carrizal fault. Based on the possible small offshore fault scarps, the Centenario fault grew northward into the La Paz Bay. At the same time, the offshore Carrizal fault appears to have stepped to the now dominant onshore Carrizal fault to form the 100-km-long escarpment bounding fault system.

The present-day setting of faulting in La Paz Bay has near constant rates along the Carrizal fault at 0.1–0.2 mm/yr from at least Trench 28 onshore to the north across La Paz Bay. Based on the lower and less certain fault scarps, we presume lesser rates of faulting on the offshore Centenario fault. It is uncertain if the onshore Centenario fault is active. Note that modern microseismicity recorded since the 1995 offshore earthquakes in the La Paz region support that the Centenario fault is active in the onshore and out into La Paz Bay (Fig. 3). There is virtually no seismicity along the Carrizal fault.

If we assume that the late Quaternary Carrizal faulting rates from this study of 0.1–0.2 mm/yr, with 0.13 mm/yr as the best estimate, were constant back to 2.5 Ma, then the fault had 325 m of offset in that last stage. If we speculate that the faulting rate was higher at ~0.5 mm/yr from 2.5 to 6–8 Ma, then the total offset would be 2–3 km, which is a reasonable geometry for a large normal fault in La Paz Bay (Fig. 12 cross section).

CONCLUSIONS

(1) The mapped onshore Carrizal fault west of La Paz and multiple likely fault scarps in the offshore in La Paz Bay suggest that the Carrizal fault is one, ~100-km-long normal fault that bounds the rift escarpment.

(2) The Carrizal fault lies 8–10 km east of the escarpment in La Paz Bay and runs along the escarpment in the onshore.

(3) Uplifted marine terraces along the west side of La Paz Bay (footwall of the fault) show a widespread record for the MIS 5e terrace at 22 m elevation, and smaller terrace remnants back to the MIS 11 terrace.

(4) Rates of faulting from two trenches onshore and uplifted marine terraces along the west side of La Paz Bay are consistent and indicate 0.1–0.2 mm/yr since ~500 ka, and a favored rate of 0.13 mm/yr since 128 ka based on marine terraces.

(5) The MRE in the two trenches indicates fault offsets of 1–2 m and suggest that the MRE may have occurred between 9 and 17 ka as a ~M 6.3–6.9 earthquake.

(6) A second fault system, the Centenario fault, lies east of the Carrizal fault, and possible offshore fault scarps and modern microseismicity suggest that it extends into La Paz Bay.

(7) Based on all of our data, the history of normal faulting in the La Paz area is complex. The offshore Carrizal fault is likely to be the oldest fault in the area and may have formed in the Miocene even though the constraints are limited. The fault appears to have grown to the south to form the onshore Centenario fault. After some complex faulting changes onshore, it seems likely that the late Quaternary fault pattern is the offshore Carrizal stepping and linking to the south to the onshore Carrizal fault, while the Centenario fault grew north into La Paz Bay. The faults appear to join to the south of the city of La Paz, where they terminate.

ACKNOWLEDGMENTS

Danny Brothers, Melanie Busch, Josh Coyan, Erin DiMaggio, Megan Muretta, Alicia Santillanez, Nathan Toke, and Olaf Zielke contributed significantly to the paleoseismic trenching and neotectonic mapping. A National Science Foundation grant from the MARGINS program to Umhoefer (OCE-0505348), Arrowsmith (OCE-0505360), Kent, and Driscoll (OCE-0112058) funded this research.

REFERENCES CITED

Atwater, T., and Stock, J., 1998, Pacific–North America plate tectonics of the Neogene southwestern United State: An update: International Geology Review, v. 40, p. 375–402, doi:10.1080/00206819809465216.

Bada, J.L., 1991, Amino acid cosmogeochemistry: Biological Sciences, v. 333, p. 349–358, doi:10.1098/rstb.1991.0084.

Bronk Ramsey, C., 1995, Radiocarbon calibration and analysis of stratigraphy: The OxCal program: Radiocarbon, v. 37, p. 425–430.

Bronk Ramsey, C., 2001, Development of the radiocarbon calibration program OxCal: Radiocarbon, v. 43, p. 355–363.

Buchanan, B., 2010, Uplifted Marine Terraces and Active Faulting along Southwestern La Paz Bay, Baja California Sur, México [M.S. thesis]: Flagstaff, Arizona, Northern Arizona University, 190 p.

Busch, M.M., Arrowsmith, J.R., Umhoefer, P.J., Coyan, J. A., Maloney, S., and Martínez Gutiérrez, G., 2011, Geometry and evolution of rift-margin, normal-fault-bounded basins from gravity and geology, La Paz–Los Cabos region, Baja California Sur, Mexico: Lithosphere, v. 3, p. 110–127, doi:10.1130/L113.1.

Cowie, P.A., and Scholz, C.H., 1992, Growth of faults by accumulation of seismic slip: Journal of Geophysical Research, v. 97, p. 11,085–11,095, doi:10.1029/92JB00586.

Coyan, M.M., Arrowsmith, J.R., Umhoefer, P.J., Coyan, J.A., Kent, G., Driscoll, N., and Martínez-Gutiérrez, G., 2013, Geometry and Quaternary slip behavior of the San Juan de los Planes and Saltito Fault Zones, Baja California Sur, Mexico: Characterization of rift-margin normal faults: Geosphere, v. 9, p. 426–443, doi:10.1130/GES00806.1.

Dawers, N., and Anders, M., 1995, Displacement-length scaling and fault linkage: Journal of Structural Geology, v. 17, p. 607–614, doi:10.1016/0191-8141(94)00091-D.

DeDiego-Forbis, T., Douglas, R., Gorsline, D., Nava-Sanchez, E., Mack, L., and Banner, J., 2004, Late Pleistocene (Last Interglacial) terrace deposits, Bahia Coyote, Baja California Sur, Mexico: Quaternary International, v. 120, p. 29–40, doi:10.1016/j.quaint.2004.01.004.

DeMets, C., 1995, Reappraisal of seafloor spreading lineations in the Gulf of California: Implications for the transfer of Baja California to the Pacific plate and estimates of Pacific–North America motion: Geophysical Research Letters, v. 22, p. 3545–3548, doi:10.1029/95GL03323.

Dixon, T., Farina, F., DeMets, C., Suarez-Vidal, F., Fletcher, J., Marquez-Azua, B., Miller, M., Sanchez, O., and Umhoefer, P., 2000, New kinematic models for Pacific–North America motion from 3 Ma to present, II: Evidence for a "Baja California shear zone": Geophysical Research Letters, v. 27, p. 3961–3964, doi:10.1029/2000GL008529.

Drake, W.R., 2005, Structural analysis, stratigraphy, and geochronology of the San Jose Island accommodation zone, Baja California Sur, Mexico [M.S. thesis]: Northern Arizona University, 231 p.

Fischer, R., Galli-Olivier, C., Gidde, A., and Schwennicke, T., 1995, The El Cien Formation of southern Baja California, Mexico: Stratigraphic precisions: Newsletters on Stratigraphy, v. 32, p. 137–161.

Fleming, K., Johnston, P., Zwartz, D., Yokoyama, Y., Lambeck, K., and Chappell, J., 1998, Refining the eustatic sea-level curve since the Last Glacial Maximum using far- and intermediate-field sites: Earth and Planetary Science Letters, v. 163, p. 327–342, doi:10.1016/S0012-821X(98)00198-8.

Fletcher, J.M., and Munguía, L., 2000, Active continental rifting in southern Baja California, Mexico: Implications for plate motion partitioning and the transition to seafloor spreading in the Gulf of California: Tectonics, v. 19, p. 1107–1123, doi:10.1029/1999TC001131.

Fletcher, J.M., Kohn, B.P., Foster, D.A., and Gleadow, A.J.W., 2000, Heterogeneous Neogene cooling and exhumation of the Los Cabos block, southern Baja California: Evidence from fission-track thermochronology: Geology, v. 28, p. 107–110, doi:10.1130/0091-7613(2000)28<107:HNCAEO>2.0.CO;2.

Gallup, C., Edwards, R.L., and Johnson, R.G., 1994, The timing of high sea levels over the past 200,000 years: Science, v. 263, p. 796–800, doi:10.1126/science.263.5148.796.

Gidde, A., 1992, Sedimentology of the Miocene Cerro Colorado Member (upper part of the El Cien Formation), Baja California Sur, México: Zentralblatt fur Geologie und Paläontologie, v. 6, p. 1467–1477.

Halfar, J., 1999, Warm-temperate to sub-tropical shallow water carbonates of the southern Gulf of California and geochemistry of rhodoliths [Ph.D. dissertation]: Stanford University, 239 p.

Hausback, B.P., 1984, Cenozoic volcanic and tectonic evolution of Baja California Sur, Mexico, *in* Frizzell, V.A., ed., Geology of the Baja California Peninsula: Bakersfield, California, Pacific Section, Society of Economic Paleontologists and Mineralogists, p. 219–236.

Kaufman, D.S., and Manley, W.F., 1998, A new procedure for determining DL Amino acid ratios in fossils using reverse phase liquid chromatography: Quaternary Science Reviews, v. 17, p. 987–1000, doi:10.1016/S0277-3791(97)00086-3.

Kennedy, G.L., LaJoie, K.R., and Wehmiller, J.F., 1982, Aminostratigraphy and faunal correlations of late Quaternary marine terraces, Pacific Coast, USA: Nature, v. 299, p. 545–547, doi:10.1038/299545a0.

Lonsdale, P., 1989, Geology and tectonic history of the Gulf of California, *in* Winterer, E.L., et al., eds., The eastern Pacific Ocean and Hawaii: Boulder, Colorado, Geological Society of America, Geology of North America, v. N, p. 499–521.

Macy, J., 2005, Rotation and uplift of Carmen Island, Baja California Sur, Mexico [M.S. thesis]: Flagstaff, Northern Arizona University, 196 p.

Maloney, S., 2009, Late Quaternary faulting history of the northern El Carrizal fault, Baja California Sur, Mexico [M.S. thesis]: Flagstaff, Northern Arizona University, 126 p.

Mayer, L., and Vincent, K.R., 1999, Active tectonics of the Loreto area, Baja California Sur, México: Geomorphology, v. 27, p. 243–255, doi:10.1016/S0169-555X(98)00074-9.

Mitterer, R.M., and Kriausakul, N., 1989, Calculation of amino acid racemization ages based on apparent parabolic kinetics: Quaternary Science Reviews, v. 8, p. 353–357, doi:10.1016/0277-3791(89)90035-8.

Molnar, P. 1973, Fault plane solutions of earthquakes and direction of motion in the Gulf of California and on the Rivera Fracture Zone: GSA Bulletin, v. 84, p. 1651–1658.

Muhs, D.R., Kelsey, H.M., Miller, G.M., Kennedy, G.L., Whelan, J.F., and McInelly, G.W., 1990, Age estimates and uplift rates for Late Pleistocene marine terraces: Southern Oregon portion of the Cascadia Forearc: Journal of Geophysical Research, v. 95, p. 6685–6698, doi:10.1029/JB095iB05p06685.

Munguía, L., Gonzalez, M., Mayer, S., and Aguirre, A., 2006, Seismicity and state of stress in the La Paz-Los Cabos region, Baja California Sur, Mexico: Bulletin of the Seismological Society of America, v. 96, p. 624–636, doi:10.1785/0120050114.

Ortlieb, L., 1991, Quaternary shorelines along the northeastern Gulf of California, geochronological data and neotectonic implications: Geological Society of America. Special Paper, v. 254, p. 95–120, doi:10.1130/SPE254-p95.

Plattner, C., Malservisi, R., Dixon, T.H., LaFemina, P., Sella, G.F., Fletcher, J., and Suarez-Vidal, F., 2007, New constraints on relative motion between the Pacific Plate and Baja California microplate (Mexico) from GPS measurements: Geophysical Journal International, v. 170, p. 1373–1380, doi:10.1111/j.1365-246X.2007.03494.x.

Puchalski, M.C., 2002, Style, kinematics, and timing of major faults on Isla Espiritu Santo, Baja California Sur, Mexico [M.S. thesis]: Flagstaff, Northern Arizona University, 166 p.

Sirkin, L., Szabo, B.J., Padilla, G.A., Pedrin, S.A., and Diez, E.R., 1990, Uranium-series ages of marine terraces, La Paz península, Baja California Sur, México: Coral Reefs, v. 9, p. 25–30, doi:10.1007/BF00686718.

Stock, J.M., and Hodges, K.V., 1989, Pre-Pliocene extension around the Gulf of California and the transfer of Baja California to the Pacific plate: Tectonics, v. 8, p. 99–115, doi:10.1029/TC008i001p00099.

Sutherland, F.H., 2006, Continental rifting across the southern Gulf of California [Ph.D. thesis]: La Jolla, University of California at San Diego.

Sutherland, F.H., Kent, G.M., Harding, A.J., Umhoefer, P.J., Driscoll, N.W., Lizarralde, D., Fletcher, J.M., Axen, G.J., Holbrook, W.S., González-Fernández, A., and Lonsdale, P., 2012, Middle Miocene to early Pliocene oblique extension in the southern Gulf of California: Geosphere, v. 8, p. 752–770, doi:10.1130/GES00770.1.

Umhoefer, P.J., Dorsey, R.J., Willsey, S., Mayer, L., and Renne, P., 2001, Stratigraphy and geochronology of the Comondú Group near Loreto, Baja California Sur, Mexico: Sedimentary Geology, v. 144, p. 125–147, doi:10.1016/S0037-0738(01)00138-5.

Umhoefer, P.J., Schwenicke, T., Del Margo, M.T., Ruiz-Geraldo, G., Ingle, J.C., Jr., and McIntosh, W., 2007, Transtensional fault-termination basins: An important basin type illustrated by the Pliocene San Jose Island basin and related basins in the southern Gulf of California, Mexico: Basin Research, v. 19, p. 297–322, doi:10.1111/j.1365-2117.2007.00323.x.

Wehmiller, J.F., and Miller, G.H., 2000, Aminostratigraphic dating methods in Quaternary geology, *in* Noller, J.S., Sowers, J.M., and Lettis, W.R., eds., Quaternary geochronology: methods and applications: Washington, D.C., American Geophysical Union, p. 187–222.

Wells, D.L., and Coppersmith, K.J., 1994, New empirical relationships among magnitude, rupture length, rupture width area, and surface displacement: Bulletin of the Seismological Society of America, v. 84, p. 974–1002.